Untersuchung von „grid cell“-basierten Repräsentationen des entorhinalen Kortex in Erwachsenen mit genetisch erhöhtem Risiko für Morbus Alzheimer

Inaugural-Dissertation

zur Erlangung des Doktorgrades

der Hohen Medizinischen Fakultät

der Rheinischen Friedrich-Wilhelms-Universität

Bonn

Lukas Herbert Otto Kunz

aus Bonn

2017

Angefertigt mit der Genehmigung

der Medizinischen Fakultät der Universität Bonn

1. Gutachter: PD Dr. rer. nat. Jürgen Fell
2. Gutachter: Prof. Dr. med. Henning Boecker

Tag der Mündlichen Prüfung: 17.10.2017

Aus der Klinik für Epileptologie

Direktor: Prof. Dr. med. Christian E. Elger (FRCP)

Inhaltsverzeichnis

1. Deutsche Zusammenfassung

Untersuchung von „grid cell“-basierten Repräsentationen des entorhinalen Kortex in Erwachsenen mit genetisch erhöhtem Risiko für Morbus Alzheimer

1.1 Einleitung

Die Alzheimer-Erkrankung (Morbus Alzheimer) ist die häufigste Form der Demenz, an der im Jahr 2010 weltweit mehr als 35 Millionen Menschen litten und die innerhalb von drei bis neun Jahren nach Diagnosestellung zum Tod führt (Querfurth & LaFerla, 2010). Die Alzheimer-Erkrankung lässt sich in eine familiäre, früh beginnende Form (Eintrittsalter 50-65 Jahre) und eine sporadische, spät beginnende Form (Erkrankungsbeginn typischerweise nach dem 65. Lebensjahr) untergliedern. Während die familiäre, früh beginnende Form vorrangig durch Mutationen in drei bestimmten Genen verursacht wird (*APP*, *PSEN1* und *PSEN2*; Blennow et al., 2006), handelt es sich bei der sporadischen, spät beginnenden Alzheimer-Erkrankung um eine multifaktoriell bedingte Erkrankung. Die vorliegende Arbeit bezieht sich grundsätzlich auf die sporadische, spät beginnende Alzheimer-Erkrankung, die den Großteil (ca. 95 %) der Alzheimer-Erkrankungen ausmacht. Klinisch zeigen sich kognitive Symptome wie Gedächtnisstörungen, Wortfindungsstörungen, Orientierungsstörungen und Werkzeugstörungen, sowie nicht-kognitive Symptome wie Depressivität, Aggressivität und paranoide Ideen. Zu den diagnostischen Kriterien der Alzheimer-Erkrankung gehören auf der einen Seite eine Beeinträchtigung des Gedächtnisses sowie auf der anderen Seite eine kognitive Dysfunktion in einem der Bereiche Sprache, Motorik, Aufmerksamkeit, Persönlichkeit und Objekterkennnung (Burns & Iliffe, 2009). Die Erkrankung beginnt schleichend und verläuft progredient. Zusätzlich können für die Diagnostik eine Liquorpunktion (erhöhtes Gesamt-Tau, vermindertes Amyloid β), CT und MRT (Atrophie insbesondere des Temporallappens), PET (temporoparietaler Hypometabolismus) und neuropsychologische Testungen (verminderter Punktewert im Mini-Mental-Status-Test und im Uhrentest) herangezogen werden. Eine definitive Diagnose der Alzheimer-Erkrankung lässt sich aktuell allerdings erst post mortem durch eine neuropathologische Untersuchung stellen. Zwei neuropathologische Veränderungen sind hierbei von entscheidender Bedeutung: Amyloid-Plaques und neurofibrilläre Tangles (Ballard et al., 2011).

Neurofibrilläre Tangles beinhalten gepaarte helikale Filamente, die aus hyperphosphorylierten Mikrotubulus-assoziierten tau-Proteinen gebildet werden (Strittmatter et al., 1994). Kurative Therapiemöglichkeiten der Alzheimer-Erkrankung stehen bislang aus (Citron, 2010), möglicherweise da potenziell wirksame Therapeutika erst zu spät im Verlauf der Erkrankung verabreicht werden (Sperling et al., 2011), wobei die frühen Stadien der Alzheimer-Erkrankung nur schwer zu diagnostizieren sind.

Daraus folgend war das Ziel der vorliegenden Arbeit, einen Beitrag zur Etablierung möglicher Früherkennungsmerkmale der Alzheimer-Erkrankung zu liefern. Um einen möglichst frühen Biomarker der Alzheimer-Erkrankung ausfindig zu machen, wurde von den etablierten Forschungserkenntnissen Gebrauch gemacht, dass (i) das ε4-Allel des *APOE*-Gens die wichtigste genetische Determinante der Alzheimer-Erkrankung ist (Corder et al., 1993), (ii) frühe neuropathologische Veränderungen der Alzheimer-Erkrankung sich im entorhinalen Kortex zeigen (Braak & Braak, 1991; Braak & Del Tredici, 2011), und zwar insbesondere in Trägern des ε4-Allels des *APOE*-Gens (Ghebremedhin et al., 1998), und (iii) der entorhinale Kortex einen Zelltyp (sogenannte „grid cells“) beherbergt, der wichtig für räumliche Navigation ist (Hafting et al., 2005) und dessen Summensignal mittels funktioneller Magnetresonanztomographie (fMRT) gemessen werden kann (Doeller et al., 2010). Dieses Summensignal wird nachfolgend als „grid cell“-basierte Repräsentationen bezeichnet. Aus (i) bis (iii) folgte die Forschungshypothese der vorliegenden Arbeit, dass junge Erwachsene, die Träger des *APOE* ε4-Allels sind, eine verminderte Stärke „grid cell“-basierter Repräsentationen im entorhinalen Kortex zeigen.

Im Folgenden werden detailliertere Hintergrundinformationen über die unterschiedlichen Anteile der Forschungshypothese gegeben. Die Allelausprägung des *APOE*-Gens gilt als die wichtigste genetische Determinante der Alzheimer-Erkrankung (wie bereits oben dargestellt bezieht sich die vorliegende Arbeit grundsätzlich auf die sporadische, spät beginnende Alzheimer-Erkrankung, die multifaktoriell bedingt ist). Drei Hauptallelvarianten des menschlichen *APOE*-Gens existieren: ε2, ε3 und ε4. Diese können in allen sechs möglichen Genotypen auftreten (die Häufigkeiten der Genotypen entsprechend Raber et al. (2004) werden in runden Klammern genannt): ε2/ε2 (1 %), ε2/ε3 (12 %), ε2/ε4 (4 %), ε3/ε3 (60 %), ε3/ε4 (21 %), ε4/ε4 (2 %). Träger eines ε4-Allels haben im Vergleich zu Nichtträgern des ε4-Allels

ein ca. vierfach erhöhtes Risiko, mit 75 Jahren an Morbus Alzheimer zu erkranken, und Träger zweier ε4-Allele haben ein sogar mehr als zehnfach erhöhtes Erkrankungsrisiko (Liu et al., 2013). Das ε2-Allel hingegen vermindert das Risiko für Morbus Alzheimer (Suri et al., 2013).

Expressionsprodukt des *APOE*-Gens ist das Apolipoprotein E (ApoE). Im zentralen Nervensystem wird ApoE hauptsächlich von Astrozyten produziert und dient als Transportprotein von Cholesterol, welches mittels ApoE-Rezeptoren in die Neurone aufgenommen wird (Liu et al., 2013). Die sich aus den unterschiedlichen *APOE*-Allelen ergebenden ApoE-Isoformen (ApoE2, ApoE3 und ApoE4) unterscheiden sich in ihrer Struktur und ihrer Fähigkeit, Lipide zu binden. Entscheidenderweise differieren sie zudem hinsichtlich ihrer Interaktion mit Amyloid β und dem tau-Protein. In Bezug auf Amyloid β scheint ApoE4 den Abbau nicht so effektiv wie die anderen Isoformen zu katalysieren, wodurch es zu einer verstärkten Amyloid β-Ablagerung und nachfolgend zu einer verstärkten Plaquebildung kommt (Schmechel et al., 1993; Polvikoski et al., 1995; Castellano et al., 2011). In Bezug auf tau zeigt ApoE4 eine verminderte Bindungsaffinität, was eine Hyperphosphorylierung von tau und somit die Entstehung von neurofibrillären Tangles begünstigt (Strittmatter et al., 1994). Zusammengenommen ist das *APOE* ε4-Allel und sein Expressionsprodukt ApoE4 mit negativen Konsequenzen auf die beiden entscheidenden neuropathologischen Faktoren der Alzheimer-Erkrankung assoziiert.

Entsprechend der sequentiellen topographischen Ausbreitung neurofibrillärer Tangles im Gehirn untergliedern die Braak-Stadien die Progression der Alzheimer-Erkrankung in sechs Stadien (Braak und Braak, 1991). In den frühen Stadien 1 und 2 ist die Bildung von neurofibrillären Tangles nahezu auf den entorhinalen Kortex beschränkt. In den Stadien 3 und 4 sind diese auch in den limbischen Regionen, z.B. dem Hippokampus, nachweisbar und in den Stadien 5 und 6 liegt eine ausgedehnte Beteiligung des Neokortex vor. Abnormale Depositionen neurofibrillärer Tangles im entorhinalen Kortex vergleichbar mit dem frühen Stadium 1 lassen sich bereits in jungen Erwachsenen mit einem Alter von unter 30 Jahren nachweisen (Braak & Del Tredici, 2011), insbesondere in Trägern des *APOE* ε4-Allels (Ghebremedhin et al., 1998). In der strukturellen Magnetresonanztomographie (MRT) wurde bereits gezeigt, dass junge *APOE* ε4-Träger eine verminderte kortikale Dicke des entorhinalen Kortex

aufweisen, wobei der Zusammenhang mit möglichen frühen neuropathologischen Veränderungen noch nicht aufgeklärt ist (Shaw et al., 2007).

Funktionell scheint der entorhinale Kortex eine wichtige Rolle bei räumlicher Navigation einzunehmen, wobei ein bestimmter Neuronentyp – sogenannte „grid cells“ – besonders prominent ist (Hafting et al., 2005). „Grid cells“ feuern immer dann, wenn sich ein Tier (oder Mensch) über die Eckpunkte eines aus gleichseitigen Dreiecken aufgebauten Gitters bewegt, welches auf die gesamte räumliche Umgebung projiziert werden kann. Dieser Zelltyp wird als neuronale Grundlage der sogenannten Pfadintegration angesehen, bei der es sich um eine bestimmte Art der Navigation handelt, die die aktuelle Position mittels Informationen über die vorherige räumliche Position, Bewegungsrichtung, Bewegungsdauer und Bewegungsgeschwindigkeit berechnet (McNaughton et al., 2006). Zum neuronalen Substrat räumlicher Navigation gehören weitere Zelltypen, die vorzugsweise in der hippokampalen Formation zu finden sind: u.a. (i) „place cells“, die an einer bestimmten Stelle im Raum feuern (O’Keefe & Dostrovsky, 1971; O’Keefe, 1976; Ekstrom et al., 2003), (ii) „border cells“, die in einem gewissen Abstand zu einer räumlichen Grenze feuern (Solstad et al., 2008), und (iii) „head direction cells“, deren Feuerrate durch die anguläre Ausrichtung des Tieres moduliert wird (Taube et al., 1990). Ergebnisse von Computermodellen weisen darauf hin, dass die Aktivität von „grid cells“ für die Bildung von „place cells“ relevant ist (Moser et al., 2008).

Auch im Menschen ließen sich „grid cells“ mittels intrakranieller Elektroenzephalographie (EEG)-Messungen in Epilepsie-Patienten nachweisen (Jacobs et al., 2013). Ein indirektes Korrelat von „grid cells“ (sogenannte „grid cell“-basierte Repräsentationen) kann zudem mittels fMRT detektiert werden, wenn sich gesunde Probanden wie bei einem Computerspiel in einer virtuellen Umgebung bewegen (Doeller et al., 2010). Hierzu wird das „blood oxygenation level dependent (BOLD)“-Signal, welches Messgegenstand der fMRT ist, auf sechsfache Rotationssymmetrie in Abhängigkeit von der Bewegungsrichtung des Probanden in der virtuellen Umgebung untersucht (die Analyse wird unter „Material und Methoden“ und in den „Supplementary Materials“ der wissenschaftlichen Veröffentlichung genauer beschrieben).

Zusammengenommen ergab sich als Forschungshypothese der vorliegenden Arbeit, dass die Stärke der „grid cell“-basierten Repräsentationen bei jungen Erwachsenen,

die Träger eines *APOE* ε4-Allels sind, vermindert ist. Eine solche Verminderung könnte als Biomarker der Alzheimer-Erkrankung dienen. Das Forschungsvorhaben wurde von der Ethikkommission des Universitätsklinikums Bonn befürwortet (Ref.-Nr. 218/13).

1.2 Material und Methoden

Die Untersuchungen in dieser Arbeit wurden an einer finalen Stichprobe von 75 jungen Erwachsenen in einem Alter von 18-30 Jahren durchgeführt (18 männliche *APOE* ε3/ε3-Träger, 19 weibliche *APOE* ε3/ε3-Träger, 18 männliche *APOE* ε3/ε4-Träger und 20 weibliche *APOE* ε3/ε4-Träger). Detaillierte Informationen zu allen methodischen Aspekten, welche hier nur gekürzt dargestellt werden, finden sich in den „Supplementary Materials“ der wissenschaftlichen Veröffentlichung (s. unten). Alle Probanden unterzogen sich einer *APOE*-Genotypisierung, einem strukturellen MRT-Scan und einem funktionellen MRT-Scan. Die MRT-Scans wurden am Deutschen Zentrum für Neurodegenerative Erkrankungen (DZNE), Bonn, durchgeführt. Die Datenerhebung erfolgte unter doppelter Verblindung, sodass weder Proband noch Versuchsleiter zu irgendeinem Zeitpunkt Kenntnis über den *APOE*-Genotyp des Probanden hatte. Zudem konnte zu keinem Zeitpunkt der wirkliche Name eines Probanden mit seinen experimentellen Daten in Verbindung gebracht werden.

Während der fMRT-Messung absolvierten die Probanden ein kognitives Paradigma, bei welchem sie sich wie bei einem Computerspiel in einer virtuellen Umgebung bewegten. Zu Beginn des Paradigmas wurden acht unterschiedliche Objekte an acht unterschiedlichen Positionen innerhalb der virtuellen Umgebung präsentiert und von dem jeweiligen Probanden aufgesammelt. Nachfolgend wurden über ca. 75 Minuten die Objektpositionen der unterschiedlichen Objekte wiederholt abgefragt (pro Objekt ca. 40 Abfragerunden, aufgeteilt auf sechs experimentelle Sessions à 13 Minuten). Jede einzelne Abfragerunde beinhaltete (i) die Objektpräsentation, in der der Proband über das zu erinnernde Objekt informiert wurde, (ii) die eigentliche Abfragephase, in welcher der Proband die Position des zuvor angezeigten Objekts erinnern und innerhalb der virtuellen Umgebung durch Navigation an die entsprechende Stelle anzeigen musste, (iii) das Feedback, welches in Form von fünf unterschiedlichen Smileys je nach Genauigkeit der räumlichen Gedächtnisleistung gegeben wurde, und (iv) die Re-Enkodierungsphase, während der das Objekt an seiner korrekten Stelle

angezeigt und von dieser durch den Probanden aufgesammelt werden musste, sodass eine stete Verbesserung des räumlichen Gedächtnisses über die Dauer des Experiments möglich war.

Das Navigationsverhalten der Probanden innerhalb der virtuellen Umgebung wurde mittels Matlab (2014a, TheMathWorks Inc., Massachusetts) hinsichtlich (i) der räumlichen Gedächtnisleistung (durchschnittlicher Abstand zwischen korrekter Objektposition und erinnerter Objektposition), (ii) der zentralen Navigationspräferenz (Anzahl der Bewegungszeitpunkte innerhalb des Zentrums der virtuellen Umgebung dividiert durch die Anzahl der Bewegungszeitpunkte innerhalb der Peripherie der virtuellen Umgebung), (iii) der Lernkurve über die Zeit, und (iv) mehrerer grundlegender Verhaltensmarker (Anzahl der Bewegungszeitpunkte, Cut-off-Geschwindigkeit, insgesamte Wegstrecke, insgesamte Anzahl an absolvierten Abfragerunden, durchschnittliche Dauer der Abfragephasen, durchschnittliche Dauer der Re-Enkodierungsphasen) untersucht.

Die strukturellen MRT-Daten wurden mittels der Software FreeSurfer (https://surfer.nmr.mgh.harvard.edu/) segmentiert und hierdurch sogenannte „regions of interest (ROIs)“ erhalten, die eine gezielte Untersuchung bestimmter Hirnregionen erlauben. In der vorliegenden Arbeit stand insbesondere der rechte entorhinale Kortex im Vordergrund, da zuvor vorzugsweise in dieser Hirnregion „grid cell“-basierte Repräsentationen gefunden worden waren (Doeller et al., 2010).

Die fMRT-Daten wurden mithilfe der Software SPM (http://www.fil.ion.ucl.ac.uk/spm/) zunächst präprozessiert. Hierzu gehörte (1) das „realignment“, bei welchem die einzelnen fMRT-Volumina (alle 2,6 Sekunden wurde während der fMRT-Messung ein solches fMRT-Volumen akquiriert) aneinander ausgerichtet werden und somit für Kopfbewegungen des Probanden während der fMRT-Messung korrigiert wird, (2) die „slice time correction“, bei der für die unterschiedlichen Akquisitionszeitpunkte der einzelnen 2D-Bilder innerhalb eines 3D-fMRT-Volumens korrigiert wird, (3) die Koregistrierung der fMRT-Volumina auf das strukturelle MRT-Volumen, wodurch die strukturellen ROIs auf die fMRT-Daten angewendet werden können, und (4) das „smoothing“ mittels eines Gauß-Kernels der Halbwertsbreite 6 mm, wodurch das Signal-Rausch-Verhältnis der fMRT-Daten gesteigert wird. Zum Teil wurden die fMRT-Daten in den Standardraum des Montreal Neurological Institute (MNI) normalisiert, um

neben den ROI-Analysen inferentielle Statistik über die Probanden in SPM zu ermöglichen.

Nach der Präprozessierung wurden die fMRT-Daten mittels einer Reihe sogenannter „general linear models (GLMs)“ modelliert. Grundprinzip dieser GLMs ist es, durch ausgewählte Regressoren (Prädiktoren) den Aktivitätsverlauf (im Sinne von BOLD-Signal) einzelner 3D-Bildelemente der fMRT-Volumina (Voxel) über das Experiment hinweg zu erklären. Den einzelnen Regressoren werden während der statistischen Auswertung durch die Software SPM sogenannte β-Werte zugeordnet, welche ausdrücken, in welchem Maße ein bestimmter Regressor den Aktivitätsverlauf eines bestimmten Voxels über das Experiment hinweg erklärt. An dieser Stelle soll nur näher auf die Analyse der „grid cell“-basierten Repräsentationen eingegangen werden – in den „Supplementary Materials“ der wissenschaftlichen Publikation (s. unten) sind hingegen alle Analysen detailliert dargelegt.

Für die Analyse der „grid cell“-basierten Repräsentationen werden die fMRT-Daten in zwei Hälften aufgeteilt. Der eine Teil der fMRT-Daten (Sessions 1, 3 und 5) wird dafür verwendet, die probandenspezifische anguläre Ausrichtung der Achsen der „grid cell“-basierten Repräsentationen zu bestimmen, da diese für jeden Probanden unterschiedlich und dementsprechend nicht *a priori* bekannt ist. Der zweite Teil der fMRT-Daten (Sessions 2, 4 und 6) wird anschließend dazu verwendet, die zuvor geschätzte anguläre Ausrichtung der Achsen der „grid cell“-basierten Repräsentationen zu testen. Ergibt dieser Test einen positiven Wert, so lässt sich dies als Vorhandensein von „grid cell“-basierten Repräsentationen in dem jeweiligen Probanden interpretieren.

Das GLM zur Modellierung des ersten Teils der Daten umfasste folgende Regressoren: (i) Bewegung innerhalb der virtuellen Umgebung (oberhalb der Cut-off-Geschwindigkeit) mit den beiden parametrischen Modulatoren $\sin(\alpha_t * 6)$ und $\cos(\alpha_t * 6)$, wobei α_t die Bewegungsrichtung zum Zeitpunkt t ist und die Multiplikation mit 6 für die Detektion der sechsfachen Rotationssymmetrie der potenziellen „grid cell“-basierten Repräsentationen nötig ist, (ii) Objektpräsentation zu Beginn einer jeden Abfragerunde, (iii) eigentliche Abfragephase, (iv) Feedback, nachdem der Proband an die erinnerte Objektposition innerhalb der virtuellen Umgebung gelaufen ist, (v) Re-Enkodierungsphase, (vi) Scanner-Drift, (vii) durchschnittliche Aktivierung pro Session und (viii) Kopfbewegungen des Probanden. Aus den β-Werten für die beiden

parametrischen Modulatoren $\sin(\alpha_t * 6)$ und $\cos(\alpha_t * 6)$ lässt sich anschließend die anguläre Ausrichtung der Achsen der probandenspezifischen „grid cell“-basierten Repräsentationen anhand von $\varphi = \text{atan2}(\beta 1, \beta 2)/6$ berechnen, wobei β1 der über alle Voxel des rechten entorhinalen Kortex gemittelte β-Wert für $\sin(\alpha_t * 6)$, β2 der über alle Voxel des rechten entorhinalen Kortex gemittelte β-Wert für $\cos(\alpha_t * 6)$ und atan2 die Matlab-Funktion für den Arkustangens ist.

Das GLM zur Modellierung des zweiten Teils der Daten umfasste folgende Regressoren: (i) Bewegung entlang einer der Achsen der „grid cell“-basierten Repräsentationen (innerhalb ±15° einer der Achsen der „grid cell“-basierten Repräsentationen), (ii) Bewegung nicht entlang einer der Achsen der „grid cell“-basierten Repräsentationen (mehr als ±15° von allen Achsen der „grid cell“-basierten Repräsentationen abweichend), (iii) Objektpräsentation zu Beginn einer jeden Abfragephase, (iv) eigentliche Abfragephase, (v) Feedback, nachdem der Proband an die erinnerte Objektposition innerhalb der virtuellen Umgebung gelaufen ist, (vi) Re-Enkodierungsphase, (vii) Scanner-Drift, (viii) durchschnittliche Aktivierung pro Session und (ix) Kopfbewegungen des Probanden. Die probandenspezifischen „grid cell“-basierten Repräsentationen ergeben sich nachfolgend aus den über alle Voxel im rechten entorhinalen Kortex gemittelten Differenzen der β-Werte für Bewegung entlang einer der Achsen der „grid cell“-basierten Repräsentationen und der β-Werte für Bewegung nicht entlang einer der Achsen der „grid cell“-basierten Repräsentationen.

An diese Hauptanalyse schlossen sich einige weitere Analysen an, die hier nur summarisch aufgelistet werden, in den „Supplementary Materials“ der wissenschaftlichen Publikation jedoch detailliert dargestellt sind.

(1) Kontrollanalysen bezüglich der „grid cell“-basierten Repräsentationen. Zur Kontrolle der Spezifität der sechsfachen Rotationssymmetrie der „grid cell“-basierten Repräsentationen wurde drei-, vier-, fünf-, sieben- und achtfache Rotationssymmetrie untersucht. Zur Kontrolle der Spezifität des rechten entorhinalen Kortex wurden auch der rechte Hippokampus und die rechte Amygdala auf sechsfache Rotationssymmetrie hin getestet.

(2) Analyse der „grid cell“-basierten Repräsentationen mittels kürzerer Datenabschnitte, i.e. anhand von jeweils zwei aufeinanderfolgenden Sessions. Diese

Analyse wurde durchgeführt, um zu zeigen, dass es nicht nur aufgrund einer zeitlichen Instabilität der Achsen der „grid cell“-basierten Repräsentationen (s. unten) zu einer Verminderung der „grid cell“-basierten Repräsentationen in *APOE* ε3/ε4-Trägern kommt, sondern auch zu einer Verminderung der Stärke der „grid cell“-basierten Repräsentationen per se (in Datenabschnitten, in denen eine zeitliche Stabilität der „grid cell“-basierten Repräsentationen gegeben ist).

(3) Lineare multiple Regressionsanalyse, um Determinanten der räumlichen Gedächtnisleistung zu bestimmen. Dementsprechend wurde als abhängige Variable der durchschnittliche Abstand zwischen korrekter Objektposition und erinnerter Objektposition verwendet. Als Prädiktoren wurden in das Regressionsmodell (a) die Stärke der „grid cell“-basierten Repräsentationen, (b) die zentrale Navigationspräferenz, (c) *APOE*-Genotyp, (d) Geschlecht und (e) Alter eingeschlossen. Für die Stärke der „grid cell“-basierten Repräsentationen wurde ein positiver Zusammenhang angenommen (umso stärker die „grid cell“-basierten Repräsentationen, desto besser die räumliche Gedächtnisleistung), was bereits gezeigt worden war (Doeller et al., 2010).

(4) Analyse von Aufgaben-bezogener Aktivität. Dies wurde mit einem separaten GLM insbesondere im Hinblick auf den Hippokampus untersucht, da mehrere vorherige Studien erhöhte hippokampale Aktivität in *APOE* ε4-Trägern gezeigt hatten und angenommen wird, dass eine erhöhte neuronale Aktivität mit einer verstärkten Ablagerung von Amyloid β zusammenhängt (Jagust et al., 2011).

(5) Analyse potenziell kompensatorischer Mechanismen. Da sich ein negativer Zusammenhang zwischen hippokampaler Aktivität und „grid cell“-basierter Repräsentationen zeigte, untersuchten wir in weiteren Analysen, ob sich durch einen positiven Zusammenhang zwischen hippokampaler Aktivität und räumlicher Gedächtnisleitung Indizien für erhöhte hippokampale Aktivität als einem kompensatorischen Mechanismus reduzierter „grid cell“-basierter Repräsentationen finden ließen. Dies wurde zum einen anhand weiterer linearer multipler Regressionsmodelle als auch anhand eines separaten GLMs genauer untersucht.

(6) Analyse der zeitlichen und räumlichen Stabilität der Achsen der „grid cell“-basierten Repräsentationen. Für die zeitliche Stabilität wurde die anguläre Ausrichtung der Achsen der „grid cell“-basierten Repräsentationen aus beiden Datenhälften

bestimmt und der prozentuale Anteil derjenigen Voxel berechnet, deren zweite anguläre Ausrichtung der Achsen innerhalb eines Bereichs von ±15° in Bezug auf die erste anguläre Ausrichtung der Achsen lokalisiert war. Für die räumliche Stabilität wurden die angulären Ausrichtungen der Achsen der „grid cell"-basierten Repräsentationen des ersten Teils der Daten mittels Rayleigh-Test auf zirkuläre Nicht-Uniformität über die Voxel des rechten entorhinalen Kortex untersucht. Beide Metriken (zeitliche und räumliche Stabilität) wurden auf eine mögliche Assoziation mit den „grid cell"-basierten Repräsentationen getestet.

(7) Funktionelle Konnektivität zwischen rechtem entorhinalen Kortex und rechtem, linkem sowie bilateralem Hippokampus.

An die probandenspezifischen Analysen schloss sich die jeweilige inferentielle Statistik über alle Probanden an (zum Teil in Abhängigkeit vom *APOE*-Genotyp, zum Teil unabhängig vom *APOE*-Genotyp), welche in SPSS (Version 22.0, IBM Corp., NY) oder in SPM durchgeführt wurde.

1.3 Ergebnisse

Auch die Ergebnisse werden im Folgenden gekürzt wiedergegeben. Eine detaillierte Darlegung mit den genauen statistischen Angaben findet sich in der wissenschaftlichen Veröffentlichung sowie den zugehörigen „Supplementary Materials".

Hinsichtlich der Gedächtnisleistung, der Lernkurven sowie der grundlegenden Verhaltensmarker war kein Unterschied zwischen beiden *APOE*-Genotypgruppen feststellbar. In Bezug auf die zentrale Navigationspräferenz wiesen *APOE* ε3/ε4-Träger jedoch verminderte Werte im Vergleich zu *APOE* ε3/ε3-Trägern auf.

Während *APOE* ε3/ε3-Träger signifikante „grid cell"-basierte Repräsentationen im rechten entorhinalen Kortex zeigten, waren diese in *APOE* ε3/ε4-Träger nicht vorhanden. Zudem war die Stärke der „grid cell"-basierten Repräsentationen in *APOE* ε3/ε4-Trägern im Vergleich zu *APOE* ε3/ε3-Trägern stark vermindert. Die weiteren Ergebnisse werden parallel zu der Auflistung im Methodenteil hier summarisch dargestellt.

(1) Die Kontrollanalysen in *APOE* ε3/ε3-Trägern ergaben wie erwartet eine Spezifität der sechsfachen Rotationssymmetrie, da weder eine dreifache, noch eine vier-, fünf-, sieben- oder achtfache Rotationssymmetrie zu einer signifikanten Aktivität des rechten entorhinalen Kortex führte. Zudem wurde die Spezifität des rechten entorhinalen Kortex bestätigt, da weder für den rechten Hippokampus noch für die rechte Amygdala signifikante „grid cell"-basierte Repräsentationen gefunden wurden.

(2) Die Analyse der „grid cell"-basierten Repräsentationen mittels kürzerer Datenabschnitte, i.e. anhand von jeweils zwei aufeinanderfolgenden Sessions, bestätigte das Hauptergebnis verminderter „grid cell"-basierter Repräsentationen in *APOE* ε3/ε4-Trägern im Vergleich zu *APOE* ε3/ε3-Trägern und zeigte gleichzeitig, dass die verminderte zeitliche Stabilität der Achsen der „grid cell"-basierten Repräsentationen (s. unten) nicht alleiniger Grund für die Verminderung der „grid cell"-basierten Repräsentationen war.

(3) Die lineare multiple Regressionsanalyse ergab einen positiven Zusammenhang zwischen „grid cell"-basierten Repräsentationen und räumlicher Gedächtnisleistung (umso stärker die „grid cell"-basierten Repräsentationen, desto besser die räumliche Gedächtnisleistung), einen positiven Zusammenhang zwischen zentraler Navigationspräferenz und räumlicher Gedächtnisleistung, besseres räumliches Gedächtnis in männlichen Probanden im Vergleich zu weiblichen Probanden und einen negativen Zusammenhang zwischen Alter und räumlicher Gedächtnisleistung.

(4) Die Analyse der Aufgaben-bezogenen Aktivität des Hippokampus ergab einen negativen Zusammenhang zur Stärke der „grid cell"-basierten Repräsentationen (umso geringer die Stärke der „grid cell"-basierten Repräsentationen, desto höher die hippokampale Aufgaben-bezogene Aktivität).

(5) Die Analyse der potenziell kompensatorischen Mechanismen zeigte, dass eine erhöhte Aktivität insbesondere des linken posterioren Hippokampus mit verbesserter räumlicher Gedächtnisleistung assoziiert war.

(6) Bei der Untersuchung der zeitlichen und räumlichen Stabilität der Achsen der „grid cell"-basierten Repräsentationen wurde manifest, dass die zeitlichen Stabilitätswerte in *APOE* ε3/ε4-Trägern im Vergleich zu *APOE* ε3/ε3-Trägern vermindert waren und nicht über Zufallslevel lagen (entsprechend der nicht vorhandenen „grid cell"-basierten Repräsentationen in *APOE* ε3/ε4-Trägern). Ebenso

war die Stärke der „grid cell“-basierten Repräsentationen hoch mit den zeitlichen Stabilitätswerten korreliert. Hingegen gab es keinen Genotypunterschied hinsichtlich der räumlichen Stabilität der Achsen der „grid cell“-basierten Repräsentationen und die räumlichen Stabilitätswerte waren nicht mit der Stärke der „grid cell“-basierten Repräsentationen korreliert.

(7) Bezüglich der funktionellen Konnektivität ergab sich über alle Probanden eine hohe Konnektivität zwischen rechtem entorhinalen Kortex und rechtem, linkem sowie bilateralem Hippokampus. Zudem ergab sich eine negative Korrelation zwischen den Konnektivitätswerten und den zeitlichen Stabilitätswerten über alle Probanden.

1.4 Diskussion

Die vorliegende Arbeit untersuchte den Einfluss des ε4-Allels des *APOE*-Gens, bei welchem es sich um die stärkste genetische Determinante der sporadischen, spät beginnenden Alzheimer-Erkrankung handelt, auf „grid cell“-basierte Repräsentationen des rechten entorhinalen Kortex. In der folgenden Diskussion werden die unterschiedlichen Ergebnisse der vorliegenden Arbeit reflektiert und in den wissenschaftlichen Kontext eingebettet.

„Grid cells“ stellen einen bestimmten Typ von Neuronen dar, welcher sich vorzugsweise im entorhinalen Kortex findet und der mit räumlicher Navigation in Verbindung gebracht wird: „Grid cells“ feuern immer dann, wenn sich ein Tier (oder Mensch) über die Eckpunkte eines intern generierten Gitters bewegt, welches die gesamte räumliche Umgebung in gleichseitige Dreiecke untergliedert (Hafting et al., 2005). Sie zeigen somit multiple Feuerfelder, welche in einem sehr spezifischen Muster angeordnet sind, wohingegen hippokampale „place cells“ nur ein Feuerfeld besitzen (Ekstrom et al., 2003). Während „place cells“ als neuronales Korrelat allozentrischer Navigation angesehen werden, handelt es sich bei „grid cells“ möglicherweise um das neuronale Substrat egozentrischer Pfadintegration, bei welcher die aktuelle räumliche Position vermittels Informationen über eine vorherige Position, Bewegungsrichtung, Bewegungsgeschwindigkeit und Bewegungsdauer errechnet wird. „Grid cell“-basierte Repräsentationen sind vermutlich die mittels fMRT messbare Summenaktivität von „grid cells“ (Doeller et al., 2010). In gängigen fMRT-Experimenten ist es nicht möglich, bestimmte Zellpopulationen zu detektieren –

stattdessen wird zumeist die generelle Aktivität einer Hirnregion gemessen, die aus dem Feuerverhalten ganz verschiedener Zelltypen resultiert. Dementsprechend lässt sich eine vermehrte oder verminderte Aktivierung sowie eine vermehrte oder verminderte Deaktivierung einer Hirnregion basierend auf fMRT-Daten meist nicht eindeutig interpretieren. Die in der vorliegenden Arbeit durchgeführte Untersuchung von „grid cell"-basierten Repräsentationen bietet hingegen den Vorteil, dass deren Verminderung in *APOE* ε3/ε4-Trägern unzweideutig als nachteilig eingeordnet werden kann – insbesondere, da eine positive Assoziation zwischen der Stärke der „grid cell"-basierten Repräsentationen und der räumlichen Gedächtnisleistung gezeigt werden konnte. Der Nachweis signifikant positiver „grid cell"-basierter Repräsentationen in *APOE* ε3/ε3-Trägern stellt zudem eine Replikation der Ergebnisse von Doeller et al. dar, welche bekräftigt, dass „grid cell"-basierte Repräsentationen mittels fMRT gemessen werden können (Doeller et al., 2010). Kürzlich wurden „grid cell"-basierte Repräsentationen auch mit der Imagination von räumlicher Navigation sowie der Exploration eines konzeptuellen Raumes in Verbindung gebracht (Horner et al., 2016; Bellmund et al., 2016; Constantinescu et al., 2016).

Die Verminderung der „grid cell"-basierten Repräsentationen in *APOE* ε3/ε4-Trägern bietet zum einen eine mögliche Erklärung für das Symptom räumlicher Desorientiertheit in Alzheimer-Patienten, zum anderen stellt sie einen potenziellen Biomarker für die Alzheimer-Erkrankung dar. Ersteres ist grundsätzlich plausibel, da „grid cells" als Teil des neuronalen Substrats räumlicher Navigation angesehen werden und Alzheimer-Patienten u.a. das Symptom der räumlichen Desorientiertheit aufweisen. Überraschend ist jedoch, dass das neuronale Korrelat (eines bestimmten Typs) räumlicher Navigation (i.e. Pfadintegration) bereits Jahrzehnte vor dem klinischen Beginn der Alzheimer-Erkrankung beeinträchtigt zu sein scheint. Dass diese Beeinträchtigung nicht bereits in jungen Erwachsenen zu einem sichtbaren Verhaltensdefizit führt, erklären wir mit kompensatorischen Mehraktivierungen anderen Hirnregionen (wie beispielsweise des Hippokampus), die weiter unten ausführlicher diskutiert werden. In Bezug auf das Potenzial unseres Ergebnisses verminderter „grid cell"-basierter Repräsentationen in *APOE* ε4-Trägern als Biomarker der Alzheimer-Erkrankung gilt es, Follow-ups unserer Probanden über die nächsten Jahrzehnte abzuwarten.

Die Dysfunktion des entorhinalen Kortex (im Sinne verminderter „grid cell“-basierter Repräsentationen) stellt zudem einen möglichen Erklärungsansatz für die in vorherigen *APOE*-fMRT-Studien gefundene Mehraktivierung bestimmter Hirnregionen dar. Seitdem das *APOE* ε4-Allel 1993 als wichtigste genetische Determinante der Alzheimer-Erkrankung identifiziert wurde (Corder et al., 1993), wurden zahlreiche Studien zu den Effekten unterschiedlicher *APOE*-Allelkombinationen auf mittels fMRT gemessene Hirnaktivierungen durchgeführt. Hierbei ist insbesondere Bookheimer et al. hervorzuheben, welche vermehrte Aktivität in mehreren Hirnregionen (linker Hippokampus, parietale und frontale Regionen) in älteren *APOE* ε4-Trägern im Vergleich zu *APOE* ε3-Trägern zeigten (Bookheimer et al., 2000). Zudem fand sich eine Korrelation zwischen der Anzahl aktivierter Hirnregionen und der kognitiven Leistungsabnahme im Rahmen eines Follow-ups zwei Jahre nach der fMRT-Messung. Solche Mehraktivierungen in *APOE* ε4-Trägern wurden in weiteren Studien bestätigt und als kompensatorische Aktivierungen interpretiert, um bereits bestehende kognitive Defizite auszugleichen (Bondi et al., 2005; Mondadori et al., 2006; Han et al., 2007; Filippini et al., 2009; Wierenga et al., 2010; Suthana et al., 2010). Zunehmend wird angenommen, dass diese kompensatorische Mehraktivierung langfristig jedoch zu einer Zunahme der neuropathologischen Veränderungen beiträgt. So konnte beispielsweise kürzlich gezeigt werden, dass erhöhte hippokampale Aktivität nachfolgend zu stärkerer Akkumulation von Amyloid β führt (Leal et al., 2017). Auch im Mausmodell konnte ein Zusammenhang zwischen neuronaler Mehraktivität und nachfolgender Aggregation von Amyloid β festgestellt werden (Bero et al., 2011). Die vorliegende Arbeit schlägt als Grund für die vermehrte hippokampale Aktivierung in *APOE* ε4-Trägern eine entorhinale Dysfunktion vor, die der hippokampalen Mehraktivierung initial vorausgeht.

Unser Ergebnis verminderter „grid cell“-basierter Repräsentationen in *APOE* ε4-Trägern ist des Weiteren im Einklang mit neuropathologischen Studien, die neurofibrilläre Tangles bereits in jungen Probanden – insbesondere in *APOE* ε4-Trägern – zeigen (Braak et al., 2011; Ghebremedhin et al., 1998). Hier besitzt auch unser Ergebnis verminderter zeitlicher Stabilität der Achsen der „grid-cell“-basierten Repräsentationen eine gewisse Aussagekraft: Die verminderte zeitliche Stabilität (bei erhaltener räumlicher Stabilität) ist möglicherweise eher auf eine intrazelluläre Schädigung der „grid cells“ – im Sinne initialer neurofibrillärer Tangles – als auf eine extrazelluläre Schädigung – im Sinne von Amyloid-Plaques – zurückzuführen. Ein

Zusammenhang zwischen neurofibrillären Tangles und verminderter „grid cell“-Funktion konnte vor kurzem auch in einem Alzheimer-Mausmodell gezeigt werden (Fu et al., 2017). In zukünftigen Studien könnte untersucht werden, wie verminderte „grid cell“-basierte Repräsentationen mit Positronen-Emissions-Tomographie (PET)-Markern der tau-Pathologie zusammenhängen (z. B. mittels 18F-AV-1451 tau-PET; Smith et al., 2016). Für diesen Ansatz spricht auch, dass neurofibrilläre Tangles (und nicht Amyloid-Plaques) mit der Dauer und Schwere der Alzheimer-Erkrankung korrelieren (Arriagada et al., 1992; Guillozet et al., 2003).

Die vorliegende Arbeit zeigte keinen generellen Einfluss des *APOE* ε4-Allels auf die räumliche Gedächtnisleistung in jungen Erwachsenen. Dieses Ergebnis steht in partiellem Gegensatz zu dem Ergebnis, dass *APOE* ε3/ε4-Träger verminderte „grid cell“-basierte Repräsentationen zeigen, da die Datenanalysen ebenfalls eine positive Korrelation zwischen der Stärke der „grid cell“-basierten Repräsentationen und der räumlichen Gedächtnisleistung ergaben. Wir erklären diesen partiellen Gegensatz damit, dass es in *APOE* ε4-Trägern kompensatorische Hirnaktivierungen gibt, die die entorhinale Dysfunktion kaschieren. Vorherige Studien, die den Einfluss des *APOE* ε4-Allels auf kognitive Leistung untersuchten, ergaben gemischte Ergebnisse. Zum einen konnten in der Tat kognitive Leistungsdefizite in *APOE* ε4-Trägern im Vergleich zu *APOE* ε3-Trägern gefunden werden (Berteau-Pavy et al., 2007). Zum anderen konnten jedoch auch kognitive Vorteile von *APOE* ε4-Trägern gezeigt werden, die zur Hypothese führten, dass das *APOE* ε4-Allel einen Fall von antagonistischer Pleiotropie darstellt (Alexander et al., 2007; Han & Bondi, 2008; Stening et al., 2015). Bei antagonistischer Pleiotropie handelt es sich um die Eigenschaft gewisser Gene, Vorteile in jungen Individuen, jedoch Nachteile in älteren Individuen zu bewirken. Andere Studien wiederum zeigten keinerlei Einfluss des *APOE* ε4-Allels auf die kognitive Leistungsfähigkeit (z.B. Jorm et al., 2007). Möglicherweise differieren die Verhaltenseffekte des *APOE* ε4-Allels nicht nur in Abhängigkeit vom Alter, sondern auch in Abhängigkeit vom jeweiligen kognitiven Unterbereich. In einer aktuellen Studie untersuchen wir deshalb, ob es einen spezifischen Effekt des *APOE* ε4-Allels auf unterschiedliche Arten von räumlicher Navigation gibt.

In der vorliegenden Arbeit konnte dennoch ein anderer Verhaltenseffekt beim Vergleich von *APOE* ε3/ε4-Trägern und *APOE* ε3/ε3-Trägern nachgewiesen werden: *APOE* ε3/ε4-Träger zeigten eine geringere Präferenz, sich in der Mitte der virtuellen

Umgebung zu bewegen. Für diesen Befund kommen mehrere potenzielle Erklärungen in Frage: (i) *APOE* ε4-Träger könnten durch diese verminderte zentrale Navigationspräferenz versuchen, Instabilitäten der „grid cell“-basierten Repräsentationen durch einen stärkeren Einfluss der die virtuelle Umgebung einschließenden Mauer zu korrigieren, (ii) die verminderte zentrale Navigationspräferenz könnte eine gewisse Unsicherheit der *APOE* ε4-Träger widerspiegeln, sich der Pfadintegration als Navigationstyp zu bedienen, die eventuell in der Mitte der virtuellen Umgebung von größerer Relevanz ist, (iii) die von den *APOE* ε4-Trägern verwendete Navigationsstrategie könnte sich hin zu einer Antwort-basierten Navigationsstrategie verlagern, die bestimmte Assoziationen zwischen der Mauer und den in der Ferne zu sehenden Bergen verwendet, und (iv) die verminderte zentrale Navigationspräferenz könnte durch inakkurate Feuerfelder der „place cells“ in der Mitte der virtuellen Umgebung aufgrund von beeinträchtigtem „grid cell“-Input auf „place cells“ entstehen (Muessig et al., 2015). Es bedarf allerdings zukünftiger Studien, um diese potenziellen Erklärungsansätze genauer zu evaluieren.

1.5 Zusammenfassung

Die Ergebnisse der vorliegenden Arbeit zeigen, dass junge Erwachsene mit genetisch erhöhtem Risiko für die Alzheimer-Erkrankung verminderte „grid cell“-basierte Repräsentationen des rechten entorhinalen Kortex und Veränderungen im räumlichen Navigationsverhalten (verminderte zentrale Navigationspräferenz) aufweisen. Des Weiteren ergab die Arbeit, dass beide Veränderungen (verminderte „grid cell“-basierte Repräsentationen sowie verminderte zentrale Navigationspräferenz) mit schlechterem räumlichem Gedächtnis assoziiert sind. Allerdings war die Stärke der „grid cell“-basierten Repräsentationen invers mit hippokampaler Aktivität assoziiert, weshalb ein direkter Effekt des genetisch erhöhten Alzheimer-Risikos auf die räumliche Gedächtnisleistung vermutlich verborgen bleibt. Zusammengenommen legen die Ergebnisse der vorliegenden Arbeit eine Dysfunktion des entorhinalen Kortex nahe, die verhaltensrelevant ist und Jahrzehnte vor dem potenziellen Beginn der Alzheimer-Erkrankung auftritt.

1.6 Literaturverzeichnis der deutschen Zusammenfassung

Alexander DM, Williams LM, Gatt JM, Dobson-Stone C, Kuan SA, Todd EG, Schofield PR, Cooper NJ, Gordon E. The contribution of apolipoprotein E alleles on cognitive performance and dynamic neural activity over six decades. Biol Psychol 2007; 75: 229-238

Arriagada PV, Growdon JH, Hedley-Whyte ET, Hyman BT. Neurofibrillary tangles but not senile plaques parallel duration and severity of Alzheimer's disease. Neurology 1992; 42: 631-639

Ballard C, Gauthier S, Corbett A, Brayne C, Aarsland D, Jones E. Alzheimer's disease. Lancet 2011; 377: 1019-1031

Bellmund JL, Deuker L, Navarro Schröder T, Doeller CF. Grid-cell representations in mental simulation. Elife 2016; 30: 5

Bero AW, Yan P, Roh JH, Cirrito JR, Stewart FR, Raichle ME, Lee JM, Holtzman DM. Neuronal activity regulates the regional vulnerability to amyloid-β deposition. Nat Neurosci 2011; 14: 750-756

Berteau-Pavy F, Park B, Raber J. Effects of sex and APOE epsilon4 on object recognition and spatial navigation in the elderly. Neuroscience 2007; 147: 6-17

Blennow K, de Leon MJ, Zetterberg H. Alzheimer's disease. Lancet 2006; 368: 387-403

Bondi MW, Houston WS, Eyler LT, Brown GG. fMRI evidence of compensatory mechanisms in older adults at genetic risk for Alzheimer disease. Neurology 2005; 64: 501-508

Bookheimer SY, Strojwas MH, Cohen MS, Saunders AM, Pericak-Vance MA, Mazziotta JC, Small GW. Patterns of brain activation in people at risk for Alzheimer's disease. N Engl J Med 2000; 343: 450-456

Braak H, Braak E. Neuropathological stageing of Alzheimer-related changes. Acta Neuropathol 1991; 82: 239-259

Braak H, Del Tredici K. The pathological process underlying Alzheimer's disease in individuals under thirty. Acta Neuropathol 2011; 121: 171-181

Braak H, Thal DR, Ghebremedhin E, Del Tredici K. Stages of the pathologic process in Alzheimer disease: age categories from 1 to 100 years. J Neuropathol Exp Neurol 2011; 70: 960-969

Burns A, Iliffe S. Alzheimer's disease. BMJ 2009; 338: b158

Castellano JM, Kim J, Stewart FR, Jiang H, DeMattos RB, Patterson BW, Fagan AM, Morris JC, Mawuenyega KG, Cruchaga C, Goate AM, Bales KR, Paul SM, Bateman RJ, Holtzman DM. Human apoE isoforms differentially regulate brain amyloid-β peptide clearance. Sci Transl Med 2011; 3: 89ra57

Citron M. Alzheimer's disease: strategies for disease modification. Nat Rev Drug Discov 2010; 9: 387-398

Constantinescu AO, O'Reilly JX, Behrens TE. Organizing conceptual knowledge in humans with a gridlike code. Science 2016; 352: 1464-1468

Corder EH, Saunders AM, Strittmatter WJ, Schmechel DE, Gaskell PC, Small GW, Roses AD, Haines JL, Pericak-Vance MA. Gene dose of apolipoprotein E type 4 allele and the risk of Alzheimer's disease in late onset families. Science 1993; 261: 921-923

Doeller CF, Barry C, Burgess N. Evidence for grid cells in a human memory network. Nature 2010; 463: 657-661

Ekstrom AD, Kahana MJ, Caplan JB, Fields TA, Isham EA, Newman EL, Fried I. Cellular networks underlying human spatial navigation. Nature 2003; 425:184-188

Filippini N, MacIntosh BJ, Hough MG, Goodwin GM, Frisoni GB, Smith SM, Matthews PM, Beckmann CF, Mackay CE. Distinct patterns of brain activity in young carriers of the APOE-epsilon4 allele. Proc Natl Acad Sci U S A 2009; 106: 7209-7214

Fu H, Rodriguez GA, Herman M, Emrani S, Nahmani E, Barrett G, Figueroa HY, Goldberg E, Hussaini SA, Duff KE. Tau Pathology Induces Excitatory Neuron Loss, Grid Cell Dysfunction, and Spatial Memory Deficits Reminiscent of Early Alzheimer's Disease. Neuron 2017; 93: 533-541

Ghebremedhin E, Schultz C, Braak E, Braak H. High frequency of apolipoprotein E epsilon4 allele in young individuals with very mild Alzheimer's disease-related neurofibrillary changes. Exp Neurol 1998; 153: 152-155

Guillozet AL, Weintraub S, Mash DC, Mesulam MM. Neurofibrillary tangles, amyloid, and memory in aging and mild cognitive impairment. Arch Neurol 2003; 60: 729-736

Hafting T, Fyhn M, Molden S, Moser MB, Moser EI. Microstructure of a spatial map in the entorhinal cortex. Nature 2005; 436: 801-806

Han SD, Houston WS, Jak AJ, Eyler LT, Nagel BJ, Fleisher AS, Brown GG, Corey-Bloom J, Salmon DP, Thal LJ, Bondi MW. Verbal paired-associate learning by APOE genotype in non-demented older adults: fMRI evidence of a right hemispheric compensatory response. Neurobiol Aging 2007; 28: 238-247

Han SD, Bondi MW. Revision of the apolipoprotein E compensatory mechanism recruitment hypothesis. Alzheimers Dement 2008; 4: 251-254

Horner AJ, Bisby JA, Zotow E, Bush D, Burgess N. Grid-like Processing of Imagined Navigation. Curr Biol 2016; 26: 842-847

Jacobs J, Weidemann CT, Miller JF, Solway A, Burke JF, Wei XX, Suthana N, Sperling MR, Sharan AD, Fried I, Kahana MJ. Direct recordings of grid-like neuronal activity in human spatial navigation. Nat Neurosci 2013; 16: 1188-1190

Jagust WJ, Mormino EC. Lifespan brain activity, β-amyloid, and Alzheimer's disease. Trends Cogn Sci 2011; 15: 520-526

Jorm AF, Mather KA, Butterworth P, Anstey KJ, Christensen H, Easteal S. APOE genotype and cognitive functioning in a large age-stratified population sample. Neuropsychology 2007; 21: 1-8

Leal SL, Landau SM, Bell RK, Jagust WJ. Hippocampal activation is associated with longitudinal amyloid accumulation and cognitive decline. Elife 2017; 8: 6

Liu CC, Kanekiyo T, Xu H, Bu G. Apolipoprotein E and Alzheimer disease: risk, mechanisms and therapy. Nat Rev Neurol 2013; 9: 106-118

McNaughton BL, Battaglia FP, Jensen O, Moser EI, Moser MB. Path integration and the neural basis of the 'cognitive map'. Nat Rev Neurosci 2006; 7: 663-678

Mondadori CR, Buchmann A, Mustovic H, Schmidt CF, Boesiger P, Nitsch RM, Hock C, Streffer J, Henke K. Enhanced brain activity may precede the diagnosis of Alzheimer's disease by 30 years. Brain 2006; 129: 2908-2922

Moser EI, Kropff E, Moser MB. Place cells, grid cells, and the brain's spatial representation system. Annu Rev Neurosci 2008; 31: 69-89

Muessig L, Hauser J, Wills TJ, Cacucci F. A Developmental Switch in Place Cell Accuracy Coincides with Grid Cell Maturation. Neuron 2015; 86: 1167-1173

O'Keefe J, Dostrovsky J. The hippocampus as a spatial map. Preliminary evidence from unit activity in the freely-moving rat. Brain Res 1971; 34: 171-175

O'Keefe J. Place units in the hippocampus of the freely moving rat. Exp Neurol 1976; 51: 78-109

Polvikoski T, Sulkava R, Haltia M, Kainulainen K, Vuorio A, Verkkoniemi A, Niinistö L, Halonen P, Kontula K. Apolipoprotein E, dementia, and cortical deposition of beta-amyloid protein. N Engl J Med 1995; 333: 1242-1247

Querfurth HW, LaFerla FM. Alzheimer's disease. N Engl J Med 2010; 362: 329-344

Raber J, Huang Y, Ashford JW. ApoE genotype accounts for the vast majority of AD risk and AD pathology. Neurobiol Aging 2004; 25: 641-650

Schmechel DE, Saunders AM, Strittmatter WJ, Crain BJ, Hulette CM, Joo SH, Pericak-Vance MA, Goldgaber D, Roses AD. Increased amyloid beta-peptide deposition in cerebral cortex as a consequence of apolipoprotein E genotype in late-onset Alzheimer disease. Proc Natl Acad Sci U S A 1993; 90: 9649-9653

Shaw P, Lerch JP, Pruessner JC, Taylor KN, Rose AB, Greenstein D, Clasen L, Evans A, Rapoport JL, Giedd JN. Cortical morphology in children and adolescents with different apolipoprotein E gene polymorphisms: an observational study. Lancet Neurol 2007; 6: 494-500

Smith R, Puschmann A, Schöll M, Ohlsson T, van Swieten J, Honer M, Englund E, Hansson O. 18F-AV-1451 tau PET imaging correlates strongly with tau neuropathology in MAPT mutation carriers. Brain 2016; 139: 2372-2379

Solstad T, Boccara CN, Kropff E, Moser MB, Moser EI. Representation of geometric borders in the entorhinal cortex. Science 2008; 322: 1865-1868

Sperling RA, Aisen PS, Beckett LA, Bennett DA, Craft S, Fagan AM, Iwatsubo T, Jack CR Jr, Kaye J, Montine TJ, Park DC, Reiman EM, Rowe CC, Siemers E, Stern Y, Yaffe K, Carrillo MC, Thies B, Morrison-Bogorad M, Wagster MV, Phelps CH. Toward defining the preclinical stages of Alzheimer's disease: recommendations from the National Institute on Aging-Alzheimer's Association workgroups on diagnostic guidelines for Alzheimer's disease. Alzheimers Dement 2011; 7: 280-292

Stening E, Persson J, Eriksson E, Wahlund LO, Zetterberg H, Söderlund H. Apolipoprotein E ϵ4 is positively related to spatial performance but unrelated to hippocampal volume in healthy young adults. Behav Brain Res 2016; 299: 11-18

Strittmatter WJ, Saunders AM, Goedert M, Weisgraber KH, Dong LM, Jakes R, Huang DY, Pericak-Vance M, Schmechel D, Roses AD. Isoform-specific interactions of apolipoprotein E with microtubule-associated protein tau: implications for Alzheimer disease. Proc Natl Acad Sci U S A 1994; 91: 11183-11186

Suri S, Heise V, Trachtenberg AJ, Mackay CE. The forgotten APOE allele: a review of the evidence and suggested mechanisms for the protective effect of APOE ε2. Neurosci Biobehav Rev 2013; 37: 2878-2886

Suthana NA, Krupa A, Donix M, Burggren A, Ekstrom AD, Jones M, Ercoli LM, Miller KJ, Siddarth P, Small GW, Bookheimer SY. Reduced hippocampal CA2, CA3, and dentate gyrus activity in asymptomatic people at genetic risk for Alzheimer's disease. Neuroimage 2010; 53: 1077-1084

Taube JS, Muller RU, Ranck JB Jr. Head-direction cells recorded from the postsubiculum in freely moving rats. II. Effects of environmental manipulations. J Neurosci 1990; 10: 436-447

Wierenga CE, Stricker NH, McCauley A, Simmons A, Jak AJ, Chang YL, Delano-Wood L, Bangen KJ, Salmon DP, Bondi MW. Increased functional brain response during word retrieval in cognitively intact older adults at genetic risk for Alzheimer's disease. Neuroimage 2010; 51: 1222-1233

2. Wissenschaftliche Veröffentlichung

Nachfolgend ist die wissenschaftliche Veröffentlichung, die 2015 in der Fachzeitschrift „Science“ publiziert wurde, angehängt.

background, SHR generated additional ground tissue layers, as previously described (*7*, *9*). However, when expressed in combinations of mutants involving *blj jkd* and *scr*, SHR failed to rescue the formative cell divisions within the ground tissue. These results indicate that BLJ, JKD, and SCR are essential for SHR to carry out ground tissue patterning. Furthermore, analysis of the contribution of the BIRDs and SCR to generate specific gene expression patterns showed that these transcription factors were able to activate expression of endodermis and cortex genes (Fig. 4C). Staining for endodermis-specific attributes (the Casparian strip) in the *shr* J0571xUAS lines showed that BLJ (Fig. 4, D to F), along with the other BIRDs and SCR (fig. S7, M to Q), could induce Casparian strip formation subsequent to periclinal divisions of the ground tissue. Expression of cortex-specific markers required at least JKD, MGP, and NUC (Fig. 4, G and H). SCZ, which is required for expression of some cortex-specific markers (*15*), is also a target in the network. Our analysis suggests that cortex identity requires multiple inputs from the BIRDs. Therefore, the BIRDs and SCR, in addition to mediating SHR transcriptional competence (*7*), are endogenous effectors of ground tissue patterning and can provide all the necessary information for the asymmetric divisions that are activated by SHR to pattern the ground tissue.

Cell fate choices in all multicellular organisms are governed by transcription factors. Their combinatorial expression and interactions are key to tissue identity. The BIRDs and SCR play critical roles in maintaining ground tissue identity in postembryonic roots by specifying the CEI stem cells that generate the ground tissue lineage (Fig. 4I). In addition, they are effectors of asymmetric divisions that pattern the progeny of the CEIs (Fig. 4J). The continuous control of multiple steps of tissue formation by the same set of transcription factors, independently of and dependent on positional cues, is a sophisticated mechanism ensuring plasticity in the regulation of cell fate.

REFERENCES AND NOTES

1. J. J. Petricka, J. M. Van Norman, P. N. Benfey, *Cold Spring Harb. Perspect. Biol.* **1**, a000497 (2009).
2. D. Welch *et al.*, *Genes Dev.* **21**, 2196–2204 (2007).
3. H. Cui *et al.*, *Science* **316**, 421–425 (2007).
4. A. Cruz-Ramírez *et al.*, *Cell* **150**, 1002–1015 (2012).
5. R. Sozzani *et al.*, *Nature* **466**, 128–132 (2010).
6. M. P. Levesque *et al.*, *PLOS Biol.* **4**, e143 (2006).
7. Y. Long *et al.*, *Plant Cell* **27**, 1185–1199 (2015).
8. R. Zhou, L. M. Benavente, A. N. Stepanova, J. M. Alonso, *Plant J.* **66**, 712–723 (2011).
9. Y. Helariutta *et al.*, *Cell* **101**, 555–567 (2000).
10. M. Pernas, E. Ryan, L. Dolan, *Curr. Biol.* **20**, 818–823 (2010).
11. M. Aida *et al.*, *Cell* **119**, 109–120 (2004).
12. V. Willemsen *et al.*, *Dev. Cell* **15**, 913–922 (2008).
13. Materials and methods are available as supplementary materials on *Science* Online.
14. S. M. Brady *et al.*, *Science* **318**, 801–806 (2007).
15. C. A. ten Hove *et al.*, *Curr. Biol.* **20**, 452–457 (2010).

ACKNOWLEDGMENTS

This work was supported by grants from the NIH (R01-GM043778) and the Gordon and Betty Moore Foundation (GBMF3405) to P.N.B.; from the NSF (IOS-1021619-002) to U.O. and P.N.B.; and from MINECO, FEDER/EFDR (BFU2013-41160-P), and FP7 (PCIG11-GA-2012-322082) to M.A.M.-R. M.A.M.-R is supported by the Ramon y Cajal program (MINECO), C.M.W. by a NRSA F32 GM106690-01 fellowship, I.B. by a NWO VIDI grant, and B.S. by an ERC Advanced Grant SysArc. J.J.P. was supported by a NIH Ruth L. Kirschstein NRSA F32 GM086976 fellowship I.B. by a NWO VIDI grant, and B.S. by an ERC Advanced Grant SysArc. We thank D. R. McClay, D. M. Pernas, and Y. Long for critical reading of the manuscript. Additional data are in the supplementary materials. The National Center for Biotechnology Information Gene Expression Omnibus accession numbers are GSE60157 (microarrays) and GSE60011 (ChIP-Seq). The authors declare that they have no competing interests.

SUPPLEMENTARY MATERIALS

www.sciencemag.org/content/350/6259/426/suppl/DC1
Materials and Methods
Figs. S1 to S7
Table S1 to S6
References (*16*–*30*)

30 July 2015; accepted 22 September 2015
10.1126/science.aad1171

ALZHEIMER'S DISEASE

Reduced grid-cell–like representations in adults at genetic risk for Alzheimer's disease

Lukas Kunz,[1,2] Tobias Navarro Schröder,[3] Hweeling Lee,[1] Christian Montag,[4] Bernd Lachmann,[4] Rayna Sariyska,[4] Martin Reuter,[5,6] Rüdiger Stirnberg,[1] Tony Stöcker,[1] Paul Christian Messing-Floeter,[1,2] Juergen Fell,[2] Christian F. Doeller,[3]* Nikolai Axmacher[1,2,7]*†

Alzheimer's disease (AD) manifests with memory loss and spatial disorientation. AD pathology starts in the entorhinal cortex, making it likely that local neural correlates of spatial navigation, particularly grid cells, are impaired. Grid-cell–like representations in humans can be measured using functional magnetic resonance imaging. We found that young adults at genetic risk for AD (*APOE*-ε4 carriers) exhibit reduced grid-cell–like representations and altered navigational behavior in a virtual arena. Both changes were associated with impaired spatial memory performance. Reduced grid-cell–like representations were also related to increased hippocampal activity, potentially reflecting compensatory mechanisms that prevent overt spatial memory impairment in *APOE*-ε4 carriers. Our results provide evidence of behaviorally relevant entorhinal dysfunction in humans at genetic risk for AD, decades before potential disease onset.

Late-onset AD is the most common form of dementia and one of the most challenging diseases of modern society (*1*). Curative therapies are still lacking, presumably because they start too late (*2*). Therefore, the elucidation of early pathomechanisms underlying symptoms of AD is of high interest. We aimed at identifying one of the potentially earliest neurocognitive pathomechanisms in the development of AD symptoms: We hypothesized entorhinal dysfunction in young *APOE*-ε4 carriers. Our hypothesis was built on three previous findings: First, the ε4 allele of the *APOE* gene is the strongest genetic risk factor for late-onset AD (*3*). Individuals carrying one *APOE*-ε4 allele are at threefold increased risk of AD, and those carrying two *APOE*-ε4 alleles are at more than 10-fold increased risk (*4*). Second, early AD histopathology appears in the entorhinal cortex (EC) (*5*), where tau abnormalities can already be observed in adults under the age of 30 (*6*), especially in *APOE*-ε4 carriers (*7*). Third, the EC contains grid cells, a cell type involved in spatial navigation. Grid cells fire whenever animals (*8*) or humans (*9*) traverse the vertices of an internally generated grid tiling the spatial environment into equilateral triangles. Their function has been linked to path integration (*10*, *11*), error correction (*12*), and the maintenance of place cells (*13*), which exhibit only a singular firing field (*14*). Hence, a possible dysfunction of grid cells may provide an explanation for the symptom of spatial disorientation in patients suffering from AD. Proxies for grid cells, termed grid-cell–like representations, are detectable in humans by functional magnetic resonance imaging (fMRI). The blood oxygenation level–dependent signal of the EC depends on movement direction with sixfold rotational symmetry. More specifically, the contrast of brain activity during movements aligned versus misaligned to the main axes of a putative grid in a virtual arena leads to a macroscopically visible fMRI signal in the right EC (*15*).

We examined the effect of *APOE*-ε4 on grid-cell–like representations by comparing two groups of healthy young adults (n = 38 *APOE*-ε4/ε3 carriers, termed "risk participants" from now on; n = 37 ε3/ε3 carriers, "control participants"; table S1). Participants completed a previously established

[1]German Center for Neurodegenerative Diseases (DZNE), Bonn, Germany. [2]Department of Epileptology, University of Bonn, Bonn, Germany. [3]Donders Institute for Brain, Cognition and Behaviour, Radboud University, Nijmegen, Netherlands. [4]Department of Psychology, Ulm University, Ulm, Germany. [5]Department of Psychology, University of Bonn, Bonn, Germany. [6]Center for Economics and Neuroscience, University of Bonn, Bonn, Germany. [7]Department of Neuropsychology, Institute of Cognitive Neuroscience, Ruhr-University Bochum, Bochum, Germany. *These authors contributed equally to this work. †Corresponding author. E-mail: nikolai.axmacher@rub.de

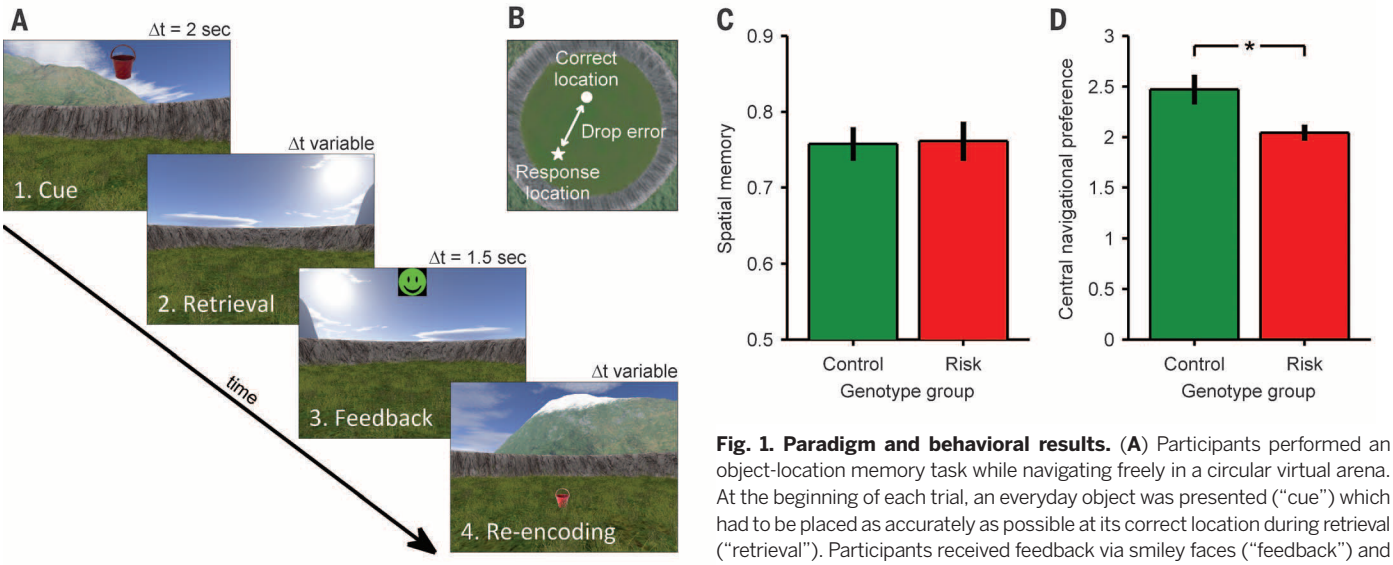

Fig. 1. Paradigm and behavioral results. (**A**) Participants performed an object-location memory task while navigating freely in a circular virtual arena. At the beginning of each trial, an everyday object was presented ("cue") which had to be placed as accurately as possible at its correct location during retrieval ("retrieval"). Participants received feedback via smiley faces ("feedback") and re-encoded the object position afterward ("re-encoding"). Δ*t*, time for specific trial phase. (**B**) For each participant, the drop error was calculated as the difference between response locations and correct locations averaged across trials. To improve readability, drop error values were transformed into spatial memory performance values (methods). (**C**) Spatial memory performance does not differ between control (*APOE*-ε3/ε3; $n = 37$) and risk (*APOE*-ε4/ε3; $n = 38$) participants. (**D**) Risk participants show a reduced preference to navigate within the arena center as compared to control participants. All bars show mean and standard error of the mean (SEM) across participants. *$P < 0.05$.

paradigm for the detection of grid-cell–like representations (*15*), during which they performed an object-location memory task while navigating freely in a virtual environment (Fig. 1 and figs. S1 and S2). Briefly, the analysis split the fMRI data into two halves (Fig. 2 and tables S4 and S5): The first half served to identify the angular orientation of the putative grid axes (separated by angles of 60°, which is equivalent to the sixfold rotational symmetry of the grid) relative to the environment in each participant's right EC (*16*). The second half of the data was then used to contrast brain activity during movements aligned with these grid axes versus brain activity during misaligned movements. The averaged contrast values of aligned versus misaligned movements across all voxels in the right EC reflect the magnitude of grid-cell–like representations [exemplary participant-specific EC region of interest (ROI); Fig. 2D]. We found significant grid-cell–like representations in control participants ($t_{36} = 2.318$, $P = 0.026$) but not in risk participants ($t_{37} = -1.730$, $P = 0.092$). In fact, the magnitude of grid-cell–like representations was strongly reduced in risk participants as compared to control participants [$t_{73} = 2.875$, $P = 0.005$; Fig. 2; two-way genotype × sex analysis of variance (ANOVA): main effect of genotype, $F_{1,71} = 8.695$, $P = 0.004$; no main effect of sex, $F_{1,71} = 0.709$, $P = 0.403$; no interaction, $F_{1,71} = 1.838$, $P = 0.179$]. Control analyses showed that our finding in control participants was specific for sixfold rotational symmetry and specific for the right EC (fig. S3). No structural changes of the right EC, which could potentially account for the functional changes, were observed (fig. S4).

In contrast to the genotype effect on grid-cell–like representations, both genetic subgroups showed similar spatial memory performance ($t_{73} = -0.109$, $P = 0.913$; Fig. 1) as well as similar basic behavioral characteristics (table S2). We assume that the detrimental effect of *APOE*-ε4 on spatial memory becomes apparent only at older age (*17*), when histopathological changes due to presymptomatic AD have reached adjacent limbic regions such as the hippocampus. However, risk participants exhibited altered navigational behavior. They showed a reduced preference to navigate in the center of the arena ("central navigational preference"; methods) as compared to control participants ($t_{73} = 2.551$, $P = 0.014$; Fig. 1 and fig. S1; two-way genotype × sex ANOVA: main effect of genotype, $F_{1,71} = 6.293$, $P = 0.014$; no main effect of sex, $F_{1,71} = 0.094$, $P = 0.761$; no interaction, $F_{1,71} = 1.978$, $P = 0.164$). This finding was also reflected in a greater mean distance of all virtual positions relative to the arena center in risk participants ($t_{73} = -3.003$, $P = 0.004$; fig. S5).

Next, we examined whether the *APOE*-dependent changes of grid-cell–like representations and central navigational preference were related to spatial memory performance. Using linear multiple regression (Table 1), we found that greater grid-cell–like representations (in addition to higher values of central navigational preference, younger age and male sex) were positively related to spatial memory performance (supplementary text and fig. S6). This result strengthens the hypothesis that EC-specific representations of space guide behavior in humans (*15*, *18*). Nevertheless, this result also seemed paradoxical to us: Given that *APOE*-ε4 reduces grid-cell–like representations and that reduced grid-cell–like representations are associated with impaired spatial memory performance, how can we explain similar performance between both genetic subgroups? Therefore, we hypothesized that there are compensatory mechanisms in risk participants (*19*).

We anticipated hippocampal task-related activity to be a compelling option for a potential compensatory mechanism because the importance of the hippocampus for spatial memory is well established (*20*), and hippocampal activity is altered in *APOE*-ε4 carriers (*21*). Hippocampal task-related activity (contrast of task versus implicit baseline; methods and table S6) was negatively correlated with grid-cell–like representations across all participants (bilateral hippocampus: Pearson's $r = -0.317$, $P = 0.006$; Fig. 2; right hippocampus: $r = -0.292$, $P = 0.011$; left hippocampus: $r = -0.320$, $P = 0.005$). Particularly in the posterior hippocampus, which is especially relevant for spatial navigation [the bilateral posterior third; see (*22*)], this relationship was significantly more pronounced in risk participants than in control participants (risk participants: $r = -0.545$, $P < 0.001$; control participants: $r = -0.064$, $P = 0.707$; difference between correlation coefficients, $z = -2.27$, $P = 0.023$; fig. S7). Because reduced grid-cell–like representations were also correlated with increased task-related activity of the EC and amygdala (fig. S8), we then examined the behavioral relevance of hippocampal task-related activity. Detailed analyses revealed that increased task-related activity, particularly in the left posterior hippocampus, was associated with better spatial memory performance (supplementary text, tables S3 and S7, and fig. S9). In short, increased hippocampal activity could serve as a behaviorally relevant compensatory mechanism for reduced grid-cell–like representations. Nevertheless, increased hippocampal activity may also indicate a broader disruption of medial temporal lobe computations promoting pathological processes [(*23*, *24*); for further discussion, see the supplementary text].

Next, we aimed at understanding the reduction of grid-cell–like representations in risk participants in greater detail. In principle, reduced grid-cell–like representations in fMRI could be due to (i) temporal instability of the putative grid axes across the entire experiment, (ii) spatial instability of the putative grid axes within each half of the experiment, or—similar temporal and spatial stability between genetic subgroups in smaller data segments provided—(iii) a relatively weaker right EC contrast of aligned versus misaligned movements. We sought to disentangle this ambiguity by first calculating one temporal stability and one spatial stability value for each participant (methods; Fig. 3). Temporal stability values differed between genetic subgroups (t_{73} = 2.408, P = 0.019), were positively correlated with grid-cell–like representations (Pearson's r = 0.736, P < 0.001; Fig. 3B), and were also negatively correlated with hippocampal task-related activity (r = −0.311, P = 0.007). Reduced temporal stability values were related to decreased functional connectivity between the right EC and hippocampus, possibly indicating a decoupling of both regions associated with entorhinal dysfunction (r = 0.298, P = 0.009; supplementary text and fig. S10). In contrast, spatial stability values did not differ between genetic subgroups and were not related to the grid-cell–like representations (t_{73} = −0.143, P = 0.887; r = −0.079, P = 0.501; Fig. 3). Finally, to disentangle reduced grid-cell–like representations from reduced temporal stability, we analyzed grid-cell–like representations on shorter data segments (methods). This analysis revealed significant grid-cell–like representations in control participants (t_{36} = 2.708, P = 0.010) but not in risk participants (t_{37} = −0.788, P = 0.436), with a significant difference between both groups (t_{73} = 2.315, P = 0.023; fig. S11), although the corresponding temporal and spatial stability values did not differ between groups (temporal stability: t_{73} = 1.459, P = 0.149; spatial stability: t_{73} = −0.421, P = 0.675). Taken together, this demonstrates that grid-cell–like representations in risk participants were less robust than in control participants (on a shorter time scale) and that the grid orientations of potential grid-cell–like representations were additionally temporally instable in risk participants (on a longer time scale).

Our results (summarized in fig. S12) support the hypothesis that AD involves the dysfunction of entorhinal grid cells. Adults at genetic risk for AD exhibit strongly reduced fMRI representations of grid cells, and reduced grid-cell–like representations are related to impaired spatial memory performance (for a speculative interpretation of the underlying mechanistic basis, see the supplementary text). We also found a reduced preference of risk participants to navigate in the center of a virtual arena. This change in navigational strategy may be interpreted (i) as an attempt to correct errors in the grid code by encounters with environmental boundaries (*25*), (ii) as an uncertainty to rely on entorhinal path integration mechanisms, (iii) as a shift toward a response-based strategy relying on different mountain-wall conjunctive features, or (iv) as a result of inaccurate place fields in the arena center due to impaired grid cell input on place cells (*26*). Moreover, our results offer an explanation for the previously observed hyperactivity of certain brain areas in *APOE*-ε4 carriers (*27*): They may compensate for entorhinal dysfunction. Specifically, our data would be in line with behaviorally relevant compensatory hyperactivity of the hippocampus that could indicate a stronger hippocampus-dependent boundary-based strategy (*28*) or enhanced hippocampal path integration computations (*29*, *30*) to counter impaired entorhinal path integration. Such neuronal hyperactivity could cause partial benefits at a young age (*31*) but may induce further pathological spreading afterward (*24*), including the degradation of place cell firing, which has already been shown in a mouse model of AD (*32*). Thus, the increased hippocampal activation may also reflect an adverse condition. Our results could provide a

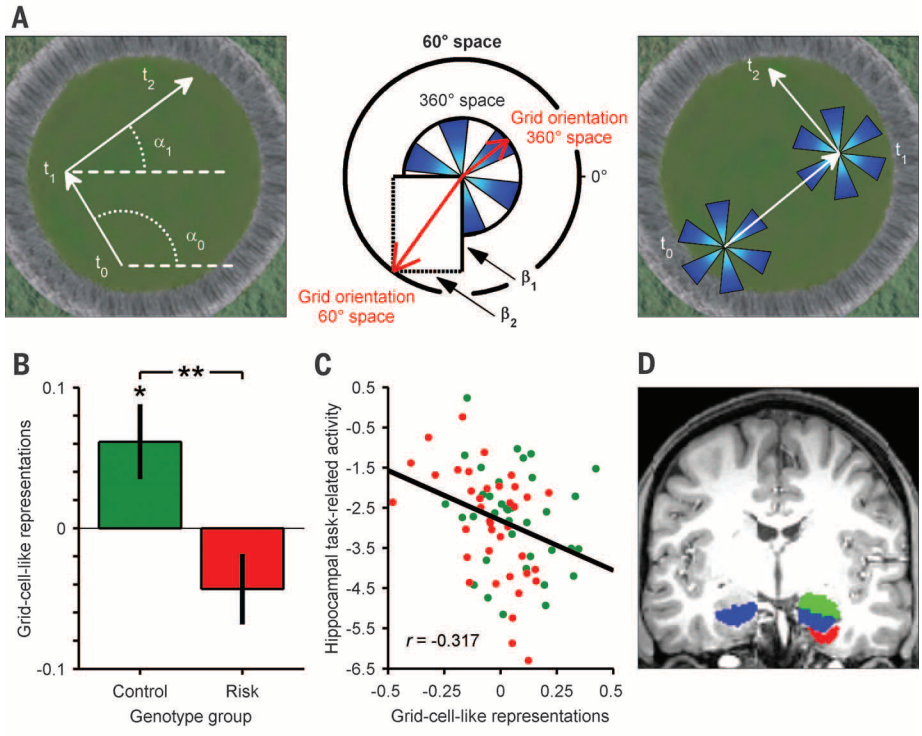

Fig. 2. Grid-cell–like representations and compensatory hippocampal activity. (**A**) Analysis procedure. (Left) The first half of the data was modeled with a general linear model (GLM), including one regressor for movement in the virtual arena. Two parametric modulators model movement direction in 60° space (sixfold rotational symmetry). *t*, time; α, running angle. (Middle) The putative grid orientation in 60° space is calculated via the β values of these parametric modulators (β_1 and β_2). Dividing by 6 yields the grid orientation in 360° space. Blue areas depict resulting aligned bins. (Right) Fitting a new GLM to the second half of the data allows the contrast of aligned versus misaligned movements to be calculated. (**B**) Grid-cell–like representations in the right entorhinal cortex (EC) are present for control participants but not for risk participants. In fact, grid-cell–like representations are reduced for risk participants as compared to control participants. (**C**) Negative correlation of task-related hippocampal activity with the magnitude of grid-cell–like representations (P = 0.006). (**D**) Exemplary ROIs of one participant, created using Freesurfer (methods). Red, right EC; blue, bilateral hippocampus; green, right amygdala. All bars show mean and SEM across participants. Green dots represent control participants; red dots represent risk participants. Units of all contrasts are parameter estimates. *P < 0.05, **P < 0.01.

Table 1. Multiple regression to predict spatial memory performance (N = 75 participants). Adjusted coefficient of determination (R^2) = 0.170. Multicollinearity was not a concern (all variance inflation factors < 1.214).

Predictor	β	*t*	*P*
Grid-cell–like representations	0.237	2.077	0.042
Central navigational preference	0.236	2.130	0.037
Genotype (control/ risk)	0.138	1.179	0.242
Sex (male/female)	−0.282	−2.643	0.010
Age (years)	−0.306	−2.830	0.006

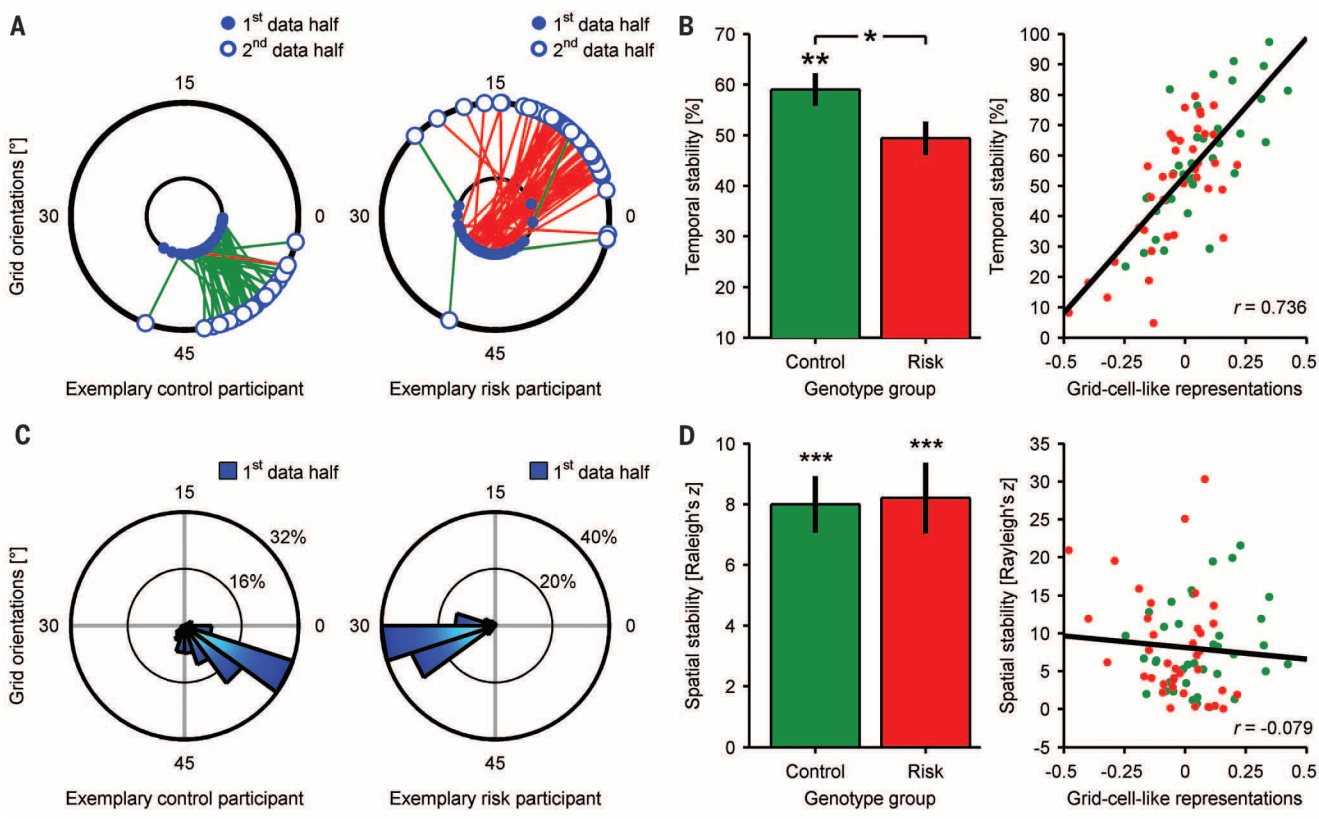

Fig. 3. Stability metrics of grid-cell–like representations. (**A**) Exemplary plots from one participant per group show temporally stable grid orientations (connected by green lines) and temporally instable grid orientations (red lines) of individual voxels, leading to one percentage value per participant ("temporal stability"). The exemplary plot for the risk participant indicates that the voxel-wise grid orientations change between the two halves of the data (lines between circles), but that within each half, the voxel-wise grid orientations are clustered (dots placed on the different circles, see spatial stability). (**B**) Temporal stability values show a reduction in risk participants and are highly correlated with grid-cell–like representations ($P < 0.001$), suggesting temporal instability as a cause of reduced grid-cell–like representations. (**C**) Exemplary plots showing spatially stable grid orientations estimated from the first half of the data (Rayleigh's $z > 11$ for both). (**D**) Contrarily to temporal stability, spatial stability values do not differ between genetic subgroups and are not related to grid-cell–like representations. All bars show mean and SEM across participants, separately for both groups. Green dots represent control participants; red dots represent risk participants. Units of all contrasts are parameter estimates. *$P < 0.05$, **$P < 0.01$, ***$P < 0.001$.

new basic framework for preclinical research on AD and may provide a neurocognitive explanation of spatial disorientation in AD. We emphasize their early occurrence in young adulthood, which may help to determine treatment onset and to establish entorhinal dysfunction as a prognostic marker. The amelioration of entorhinal dysfunction might be a new therapeutic target in the treatment of AD.

REFERENCES AND NOTES

1. H. W. Querfurth, F. M. LaFerla, *N. Engl. J. Med.* **362**, 329–344 (2010).
2. R. A. Sperling, C. R. Jack Jr., P. S. Aisen, *Sci. Transl. Med.* **3**, 111cm33 (2011).
3. E. H. Corder *et al.*, *Science* **261**, 921–923 (1993).
4. C. C. Liu, T. Kanekiyo, H. Xu, G. Bu, *Nat. Rev. Neurol.* **9**, 106–118 (2013).
5. H. Braak, E. Braak, *Acta Neuropathol.* **82**, 239–259 (1991).
6. H. Braak, K. Del Tredici, *Acta Neuropathol.* **121**, 171–181 (2011).
7. E. Ghebremedhin, C. Schultz, E. Braak, H. Braak, *Exp. Neurol.* **153**, 152–155 (1998).
8. T. Hafting, M. Fyhn, S. Molden, M. B. Moser, E. I. Moser, *Nature* **436**, 801–806 (2005).
9. J. Jacobs *et al.*, *Nat. Neurosci.* **16**, 1188–1190 (2013).
10. G. Buzsáki, E. I. Moser, *Nat. Neurosci.* **16**, 130–138 (2013).
11. M. E. Hasselmo, M. P. Brandon, *Neural Plast.* **2008**, 658323 (2008).
12. S. Sreenivasan, I. Fiete, *Nat. Neurosci.* **14**, 1330–1337 (2011).
13. D. Bush, C. Barry, N. Burgess, *Trends Neurosci.* **37**, 136–145 (2014).
14. A. D. Ekstrom *et al.*, *Nature* **425**, 184–188 (2003).
15. C. F. Doeller, C. Barry, N. Burgess, *Nature* **463**, 657–661 (2010).
16. Materials and methods are available as supplementary materials on *Science* Online.
17. F. Berteau-Pavy, B. Park, J. Raber, *Neuroscience* **147**, 6–17 (2007).
18. M. J. Chadwick, A. E. Jolly, D. P. Amos, D. Hassabis, H. J. Spiers, *Curr. Biol.* **25**, 87–92 (2015).
19. S. Y. Bookheimer *et al.*, *N. Engl. J. Med.* **343**, 450–456 (2000).
20. B. A. Strange, M. P. Witter, E. S. Lein, E. I. Moser, *Nat. Rev. Neurosci.* **15**, 655–669 (2014).
21. N. Filippini *et al.*, *Proc. Natl. Acad. Sci. U.S.A.* **106**, 7209–7214 (2009).
22. M. S. Fanselow, H. W. Dong, *Neuron* **65**, 7–19 (2010).
23. A. Bakker *et al.*, *Neuron* **74**, 467–474 (2012).
24. A. W. Bero *et al.*, *Nat. Neurosci.* **14**, 750–756 (2011).
25. K. Hardcastle, S. Ganguli, L. M. Giocomo, *Neuron* **86**, 827–839 (2015).
26. L. Muessig, J. Hauser, T. J. Wills, F. Cacucci, *Neuron* **86**, 1167–1173 (2015).
27. A. J. Trachtenberg, N. Filippini, C. E. Mackay, *Neurobiol. Aging* **33**, 323–334 (2012).
28. C. F. Doeller, J. A. King, N. Burgess, *Proc. Natl. Acad. Sci. U.S.A.* **105**, 5915–5920 (2008).
29. T. Wolbers, J. M. Wiener, H. A. Mallot, C. Büchel, *J. Neurosci.* **27**, 9408–9416 (2007).
30. K. R. Sherrill *et al.*, *J. Neurosci.* **33**, 19304–19313 (2013).
31. C. R. Mondadori *et al.*, *Cereb. Cortex* **17**, 1934–1947 (2007).
32. F. Cacucci, M. Yi, T. J. Wills, P. Chapman, J. O'Keefe, *Proc. Natl. Acad. Sci. U.S.A.* **105**, 7863–7868 (2008).

ACKNOWLEDGMENTS

The authors thank H. Boecker, V. Heise, W. Huijbers, T. Reber, and S. Remy for comments on the manuscript and A. Rühling and Y. Sagik for their help with fMRI scanning. We also thank all of the participants for their participation in this study. L.K. was supported by a Bonfor dissertation stipend of the Medical Faculty of the University of Bonn and a stipend of the German National Academic Foundation (Studienstiftung des deutschen Volkes). C.M. is funded by a Heisenberg grant awarded to him by the German Research Foundation (DFG, MO 2363/3-1). P.C.M.F. was supported by a stipend of the Konrad Adenauer Foundation (Konrad-Adenauer-Stiftung). C.F.D. and T.N.S. are supported by the European Research Council (grant ERC-StG 261177) and the Netherlands Organisation for Scientific Research (grant NWO-Vidi 452-12-009). N.A. received DFG funding from Emmy Noether grant AX82/2 and together with J.F. via the Sonderforschungsbereich 1089. The authors declare no conflicts of interest. All raw data are archived at the German Center for Neurodegenerative Diseases (DZNE), Bonn.

SUPPLEMENTARY MATERIALS

www.sciencemag.org/content/350/6259/430/suppl/DC1
Materials and Methods
Supplementary Text
Figs. S1 to S12
Tables S1 to S7
References (*33*–*62*)

17 June 2015; accepted 23 September 2015
10.1126/science.aac8128

www.sciencemag.org/content/350/6259/430/suppl/DC1

Supplementary Materials for

Reduced grid-cell–like representations in adults at genetic risk for Alzheimer's disease

Lukas Kunz, Tobias Navarro Schröder, Hweeling Lee, Christian Montag, Bernd Lachmann, Rayna Sariyska, Martin Reuter, Rüdiger Stirnberg, Tony Stöcker, Paul Christian Messing-Floeter, Juergen Fell, Christian F. Doeller, Nikolai Axmacher*

*Corresponding author. E-mail: nikolai.axmacher@rub.de

Published 23 October 2015, *Science* **350**, 430 (2015)
DOI: 10.1126/science.aac8128

This PDF file includes:

Materials and Methods

Participants and *APOE* genotyping

We recruited 531 healthy Caucasian participants in different lectures of the University of Bonn and performed genotyping by means of buccal swabs. Automatic purification of genomic DNA was conducted via the MagNA Pure® LC system using a commercial extraction kit (MagNA Pure LC DNA isolation kit; Roche Diagnostics, Mannheim, Germany). Analysis of the *APOE* polymorphisms was performed with real-time polymerase chain reaction (PCR) on a Light Cycler System by Roche. Primers and hybridization probes were provided by TIBMOLBIOL, Berlin, Germany. From this large cohort, we successively and randomly invited male and female participants (age range, 18 – 30 years) who were either homozygous for *APOE*-ε3 ("control participants") or heterozygous for *APOE*-ε4/ε3 ("risk participants") to the fMRI experiment until at least 20 participants were scanned in each of the four groups (male control, female control, male risk, and female risk). Sample sizes were based on Doeller et al. (*15*) and previous *APOE*-fMRI-studies (e.g., ref. *21*). No statistical method was used to predetermine sample size. We did not include a third genetic subgroup with homozygous *APOE*-ε4-carriers, because they were too rare ($n = 8$). Participants as well as experimenters were blinded towards genotypes. Participants' real names and genotypes were never directly connected. In total, 94 participants were scanned. Ten participants did not complete the experiment and 9 had to be excluded because of excessive head motion (more than 4 mm into one or more translational directions). Thus, all analyses were performed with a final number of $N = 75$ participants ($n = 18$ male control, $n = 19$ female control, $n = 18$ male risk, and $n = 20$ female risk). Control and risk groups did not differ in demographic characteristics (see Table S1). All participants had normal or corrected-to-normal vision and reported no history of neurological or psychiatric disease. The local Ethics Committee of the University of Bonn approved the study and all participants signed a written informed consent.

Experimental task

The paradigm was adapted from Doeller et al. (*15*). During the fMRI scan, participants performed an object-location memory task navigating freely in a circular virtual arena. The arena comprised a grassy plane (diameter of 9,500 virtual units) bounded by a cylindrical cliff. No intra-maze landmark (as used in previous versions of the task; *28*, *15*) was present. Movement in the arena was enabled using a button box with three buttons for the different movement directions (move forward, turn right, turn left) and one button for object placement. The total duration of 78 minutes was divided into 6 sessions of 13 minutes each. Sessions were separated by short breaks. At the very beginning of session 1, participants collected eight everyday objects (randomly drawn from a total number of 12 potential objects: eggplant, baby bottle, briefcase, globe, bucket, rubber duck, barrel, stapler, agenda, vase, alarm clock, basketball) from different locations in the arena ("initial learning phase"). This time period (variable duration of approximately two minutes, as the whole task was self-paced) was excluded from all analyses by removing the corresponding fMRI volumes. Object locations were randomly distributed and similarly central between the two genetic subgroups (measured as the mean distance between the object locations and the arena center; two-sample *t*-test, $t_{73} = -$

.617, $P = .539$). Several constraints ensured that the object positions were not too close to the cylindrical cliff, the center, and other objects. Afterwards, participants completed variable numbers of trials (mean number of trials ± standard error of the mean (SEM), 229 ± 5), depending on individual movement speed. Each trial consisted of a retrieval and a subsequent re-encoding phase (Fig. 1A). During the retrieval phase, participants were shown one of the eight objects ("Cue") and asked to place it as accurately as possible at its initial position ("Response location"; Fig. 1B). Depending on response accuracy, participants then received feedback via one of five possible smiley faces (Fig. S1B). Afterwards, each object had to be collected again from its initial position ("Correct location"; Fig. 1B), allowing for re-encoding. Thus, participants gradually improved their performance throughout the experiment (Fig. S2). After each trial, a fixation crosshair was shown for a variable duration of 3 to 5 sec (uniformly distributed). At the beginning of the first trial (after the initial learning phase), participants started from locations that were similarly central between the two groups (two-sample *t*-test, $t_{73} = -1.107$, $P = .272$). Subsequent starting positions of all retrieval phases were identical with the self-paced end positions of the directly preceding re-encoding phases to ensure a continuous, more natural navigation course. Note that these end positions were not completely identical with the object positions since participants only needed to enter a circle with a radius of 120 virtual units around each object to "collect" it. Every 0.1 sec, the position of the participant in the arena was logged, which allowed us to extract movement periods, movement speed and movement direction. The virtual arena was projected onto a screen positioned at the head of the magnet bore and reflected onto a mirror attached to the head coil.

MRI data acquisition

Scanning was performed at the German Center for Neurodegenerative Diseases (DZNE), Bonn, using a *Skyra* 3-T MRI scanner (Siemens, Erlangen, Germany) with a 20-channel head receive coil. Participants underwent a T1 weighted structural scan and a T2*-weighted functional scan. For T1-weighted structural brain imaging, a whole-head magnetization-prepared rapid gradient-echo imaging sequence (MP-RAGE) with the following parameters was used: 1 mm isotropic resolution; inversion time (TI) = 1100 ms; repetition time (TR) = 2500 ms; echo time (TE) = 4.37 ms; flip angle = 7°; total acquisition time (TA) = 5:08 min. Functional images were subsequently acquired using a T2*-weighted echo-planar-imaging (EPI) protocol, adapted to account for increased susceptibility-induced artifacts in inferior slices (*33*), with the following parameters: acquisition matrix = 64 x 64; TR = 2600 ms; field of view = 192 mm x 192 mm; flip angle = 82°. Forty 2 mm-thick transversal slices were acquired in ascending order (1 mm slice gap) within each TR. The anterior-posterior phase encoding direction was tilted by 30° towards the coronal plane (lifted anterior end). The echo time for superior slices was set to $TE_{max} = 31$ ms while the echo time for inferior slices was set to $TE_{min} = 23$ ms with a linear increase from the 14^{th} to the 24^{th} slice. The fMRI time series comprised six sessions, each consisting of 305 images (TA = 13:13 min per session). The first five images of each session were excluded from data analysis to account for signal steady-state transition.

Data analysis

Matlab (2014a, The MathWorks Inc., Massachusetts) was used to perform behavioral analyses. Freesurfer (v5.3.0, http://surfer.nmr.mgh.harvard.edu/) enabled the creation of participant-specific anatomical ROIs and was used to obtain four structural measures of right entorhinal cortex (volume, thickness, mean curvature, and surface area). SPM8 (http://www.fil.ion.ucl.ac.uk/spm) served to perform all first level analyses of functional MR images as well as the confirmatory second level analysis of compensatory activity on whole brain level. SPSS (version 22.0, IBM Corp., NY) was used to calculate all other second-level statistics. Most data were normally distributed and variance was similar between groups. Otherwise, non-parametric test statistics and corrections for unequal variances were chosen. All second-level statistics were two-sided.

Behavioral analyses

First, we assessed participant-specific spatial memory performance by averaging the distances between response and correct locations across trials ("drop error", Fig. 1B). Solely for visualization and enhanced readability, we converted these "drop errors" into values of spatial memory performance using the following formula: spatial memory performance$_i$ = [max(drop error) - drop error$_i$ + min(drop error)] / max(drop error), where max(drop error) and min(drop error) correspond to the maximum and minimum drop error across all participants, respectively, and drop error$_i$ corresponds to the drop error in participant *i*. This formula simply reverses the drop errors and maps them into the range between 0 and 1. Second, participant-specific values of central navigational preference were calculated as central navigational preference = n_{center} / $n_{periphery}$, where n_{center} is the number of time points spent in the center of the arena and $n_{periphery}$ is the number of time points spent in the periphery of the arena. The division between center and periphery was drawn by dividing the arena radius into two equal halves. Only time points during the retrieval phase were considered, as we expected a behavioral relevance for correct object placement solely during this trial phase. Drop error values and central navigational preference values were entered into two-sample *t*-tests between genetic subgroups. The result of the central navigational preference values was corrected for unequal variances (assessed via Levene's test for equality of variances) using the Welch-Scatterthwaite method as implemented in SPSS by default. To validate our metric of central navigational preference, we determined the absolute distances of the self-paced starting positions as well as all self-paced positions relative to the center and compared them between genetic subgroups using two-sample *t*-tests. Third, as control analyses, we calculated basic behavioral characteristics including the number of movement time points, the cut-off speed (used for the definition of fast movements, see analysis of grid-cell-like representations below), the total path length, the total number of trials, the average duration of retrieval-phases, and the average duration of re-encoding-phases. Potential differences between these characteristics as a function of genotype were tested (Table S2). Finally, learning curves were calculated across participants of both genetic subgroups. For visualization and statistical evaluation with a time × genotype repeated measures ANOVA, drop error times were assigned to one-minute-bins and corresponding drop errors averaged within bins, leading to 77 drop error values per participant (Fig. S2).

Pre-processing of functional images

SPM8 within Matlab was used to pre-process each participant's fMRI data. Functional images were spatially realigned, unwarped, slice time corrected and coregistered onto participant-specific anatomical T1 images. For the analysis of grid-cell-like representations (Fig. 2B), stability metrics (Fig. 3), and task-related activity (Fig. 2C, Fig. S8), we did not apply normalization as we exclusively performed ROI analyses and aimed at minimizing post hoc spatial distortions of the data. Only for the "confirmatory analysis of compensatory mechanisms" (see below; Fig. S9), we applied normalization to Montreal Neurological Institute (MNI) space using parameters from the segmentation of the T1 structural image (*34*). Images were spatially smoothed with an isotropic 6 mm full-width-half-maximum Gaussian kernel.

Creation of participant-specific anatomical ROIs

To improve the accuracy of the ROI analyses, normalization was replaced by the usage of participant-specific anatomical ROIs (right, left, and bilateral EC; right, left, and bilateral hippocampus; right, left, and bilateral posterior hippocampus; right, left, and bilateral amygdala; right, left, and bilateral fusiform gyrus; right, left, and bilateral precentral cortex) created via the Freesurfer image analysis suite (see Fig. 2D for exemplary ROIs of right EC, right amygdala and bilateral hippocampus). The right EC ROI was used in the analysis of grid-cell-like representations. The right hippocampal and right amygdala ROIs were used to perform control analyses in control participants as they are adjacent regions of the right EC. Finally, the other ROIs served for the analysis of task-related activity. Briefly, processing included registration to Talairach space, intensity normalization, skull stripping, volumetric labelling, and cortical parcellation. The detailed procedure has been described and validated in previous publications (*35-37*) and is comparable in accuracy to manual labelling (*38*). Afterwards, Freesurfer output was transformed back into participant-specific space to establish compatibility with the coregistered, smoothed functional images. Next, the parcellated cortical ribbon was used to obtain ROIs of EC, fusiform gyrus, and precentral cortex, whereas the segmented subcortical structures were used to produce ROIs of hippocampus and amygdala. All participants' ROIs were visually inspected by overlaying them onto the participant-specific anatomical T1 image to ensure proper definition. The number of voxels of our main target ROIs did not differ between genetic subgroups (two-sample *t*-test for right EC, $t_{73} = -1.309$, $P = .195$, mean number of voxels ± SEM: 1704 ± 60 in control participants, 1811 ± 55 in risk participants; two-sample *t*-test for bilateral hippocampus, $t_{73} = -.789$, $P = .432$, mean number of voxels ± SEM: 9062 ± 155 in control participants, 9225 ± 136 in risk participants) and were in accordance with previous findings (right EC, mean ± SEM, 1759 ± 41, see ref. *39*; bilateral hippocampus, mean ± SEM, 9144 ± 103, see ref. *40*). Furthermore, the voxel numbers of all other ROIs that were additionally used also did not differ between genetic subgroups (two-sample *t*-tests, all $P > .05$).

Analysis of grid-cell-like representations

The analysis of grid-cell-like representations followed the procedure of Doeller et al. (*15*): The data was split into two halves. By fitting a first general linear model (GLM) to the first half of the data (Fig. 2A, left panel), we identified the angular orientation of the putative grid axes relative to the environment in each participant's right EC (Fig. 2A,

middle panel; Table S4), because the angular orientation is not known a priori. Afterwards, we modeled the second half of the data with a second GLM to contrast brain activity during aligned movements with brain activity during misaligned movements relative to the previously identified putative grid axes from the first half of the data (Fig. 2A, right panel; Table S5). This procedure is explained in greater detail hereinafter. The a priori defined first half of the data (sessions 1, 3, and 5) was modeled with a first GLM including a regressor for all fast movement time points (see below) in the virtual arena and regressors of no interest modeling phases without navigation in the environment (Table S4). Two parametric modulators of the movement regressor modeled the movement direction at each movement time point: $\sin[\alpha(t) * 6]$ and $\cos[\alpha(t) * 6]$, where $\alpha(t)$ is the movement direction at time point t (Fig. 2A, left panel), arbitrarily aligned to 0° of the virtual reality environment as defined by the background cues. Multiplying by six transforms the movement directions into 60° space to account for the six-fold rotational symmetry of potential grid-cell-like representations. In other words, the factor 6 means that these regressors are sensitive to activation showing a six-fold rotational symmetry in running direction (i.e., activation with six evenly spaced peaks as a function of running direction will produce parameter estimates β_1 and β_2 for the two regressors with large amplitude $\text{sqrt}(\beta_1^2 + \beta_2^2)$). Next, the β-values of the two parametric modulators were extracted from the right EC ROI to calculate its putative mean grid orientation in 60° space (varying between -180° and 180°): mean grid orientation $\varphi_{60°} = \arctan(\beta_1/\beta_2)$, where β_1 = averaged beta value for $\sin[\alpha(t) * 6]$ and β_2 = averaged beta value for $\cos[\alpha(t) * 6]$ across voxels of the right EC ROI. Dividing by six changed the mean grid orientation $\varphi_{60°}$ back into normal 360° space (varying between -30° and 30°). Adding n times 60° yielded all putative grid axes (Fig. 2A, middle panel). Afterwards, we looked for sinusoidal modulation of activation with six-fold rotational symmetry in the other half of the data. In detail, this means that a second GLM was applied to the a priori defined second half of data (sessions 2, 4, and 6) containing regressors for "aligned" (within ± 15° of the nearest axis of the grid) and "misaligned" (more than ± 15° from a grid axis) movements in the virtual arena (Fig. 2A, right panel; Table S5). Contrast values (aligned > misaligned) were extracted from the right EC ROI and averaged across voxels within participants. More positive values indicate more pronounced grid-cell-like representations, whereas smaller or even negative values indicate less pronounced grid-cell-like representations. Please note that we restricted our analysis to the right EC and fast movements (fast tertile of all movements, separately determined for each participant, lower boundary defined as "cut-off speed", see Table S2), following Doeller et al. (*15*).

Control analyses of grid-cell-like representations

In control participants, we performed two control analyses to validate both the specificity of six-fold rotational symmetry and the specificity of the right EC ROI. To test for the specificity of the six-fold symmetric sinusoidal modulation, we used the same analysis procedure of (1) estimating the mean grid orientation of the right EC and (2) looking for sinusoidal modulation in control models, however with directional periodicities of 120°, 90°, 72°, 51.4°, and 45° (that is, three-fold, four-fold, five-fold, seven-fold, and eight-fold rotational symmetry) respectively. To test for the specificity of the right EC ROI, we performed the analysis with 6-fold rotational symmetry in right

hippocampus and right amygdala, since they are adjacent regions of the right EC (for the results, see Fig. S3).

Session-wise analysis of grid-cell-like representations

To evaluate whether grid-cell-like representations were also reduced under the conditions of similar temporal and spatial stability of the voxel-wise grid orientations between genetic subgroups, we applied the analysis of grid-cell-like representations (see above) on shorter data segments: one session served to identify the angular orientation of the putative grid axes and the subsequent session served to contrast brain activity during movements aligned with these grid axes versus brain activity during misaligned movements, leading to five session combinations (estimate grid orientation in session 1, calculate contrast of aligned versus misaligned movements in session 2; same between session 2 and session 3; session 3 and session 4; session 4 and session 5; session 5 and session 6). Temporal and spatial stability values were assessed for each session combination following the procedure explained below. The results were averaged across session combinations before entering group statistics.

Linear multiple regression to predict spatial memory performance

To investigate whether grid-cell-like representations and central navigational preference were related to spatial memory performance, we calculated a linear multiple regression model with spatial memory performance as the dependent variable. Grid-cell-like representations, central navigational preference, genotype, sex, and age were included as relevant predictor variables. Concerning grid-cell-like representations, we hypothesized a positive influence on spatial memory performance as shown before (*15*).

Analysis of task-related activity

Hippocampal task-related activations were estimated using a separate GLM including a regressor that modeled the time during which participants were engaged in the task (i.e., cue, retrieval, feedback, and re-encoding combined; Table S6). Contrast values for this regressor versus the implicit baseline were extracted from the participant-specific right, left, and bilateral hippocampal ROIs (created using Freesurfer, see above) and averaged across voxels within participants ("hippocampal task-related activation"). Afterwards, we examined whether reduced right EC grid-cell-like representations were related to increased hippocampal task-related activity across all participants by calculating a Pearson correlation. To further elucidate the relationship between grid-cell-like representations and other ROIs inside and outside the medial temporal lobe, task-related activations were also extracted from EC, amygdala, fusiform gyrus, and precentral cortex (created using Freesurfer) and correlated to the grid-cell-like representations (Fig. S8) using Pearson correlations.

Analysis of potentially compensatory mechanisms

To elucidate whether our finding of increased hippocampal task-related activity reflects compensatory mechanisms with a behavioral impact, we conducted two analyses. First, we calculated six different versions of the linear multiple regression (Table S3) used to predict spatial memory performance in the main text (Table 1). Each version included task-related activity of a different part of the hippocampus (bilateral

hippocampus, left hippocampus, right hippocampus, bilateral posterior hippocampus, left posterior hippocampus, right posterior hippocampus) as an additional independent variable. We were specifically interested in the influence of task-related activity of the posterior hippocampus, since this is the region of the hippocampus that has been shown to be especially relevant for spatial navigation (*22*, *41-45*). Second, we performed a separate second-level whole brain analysis using SPM. Here, first level contrast-images represented trial-by-trial response accuracy within participants (see below: "Confirmatory analysis of compensatory mechanisms"). See below for the results.

Confirmatory analysis of compensatory mechanisms

To validate our result of compensatory hippocampal activity, we used an additional whole-brain approach that identified voxels which were specifically relevant for correct object placement (i.e., good spatial memory performance) and that were also negatively correlated to grid-cell-like representations. This approach contained a first level GLM and a second level analysis in SPM. Hence, exclusively for this analysis, pre-processing of functional images included normalization to MNI space before smoothing. On the first level, the GLM contained one regressor of the retrieval-phase that was modeled with a parametric modulator depicting the accuracies of the trial-specific response locations (Table S7) revealing voxels associated with good spatial memory performance. Contrast images of the parametric modulator versus zero were calculated for all participants and entered into a second level linear regression model in SPM. This linear regression model contained the participant-specific grid-cell-like representations of right EC as predictor variable. We then identified voxels which were negatively correlated with grid-cell-like representations across the group of participants, also reflecting potential compensatory mechanisms. Based on our strong a priori hypothesis, we applied small volume correction (SVC) for bilateral hippocampus (SPM anatomy toolbox mask image; mask volume = 23,664 mm^3). We report activation at $P < .05$ at the peak level corrected for multiple comparisons within this search volume.

Calculation of temporal and spatial stability

Grid-cell-like representations solely occur when the voxel-wise grid orientations (angular orientation of the putative grid axes relative to the environment in 60° space) from the first half of the data exhibit both spatial and temporal stability. Thus, in principle, reduced grid-cell-like representations can be either due to spatial or temporal instability of the voxel-wise grid orientations (or – similar temporal and spatial stability between genetic subgroups in smaller data segments provided – due to a relatively weaker right EC contrast of aligned versus misaligned movements, which we investigated using shorter data segments, see main text and above: "Session-wise analysis of grid-cell-like representations"). For each participant, we calculated one spatial stability value (statistically expressed as Rayleigh's *z*-value: the higher the *z*-value, the higher spatial stability) and one temporal stability value (estimated as percentage values: the higher the percentage value, the higher temporal stability). This is explained in greater detail henceforth. Spatial instability is maximal for a uniform circular distribution of grid orientations across voxels. As a result of spatial instability, the mean grid orientation of the first half of the data would be a random selection of this distribution. Arbitrary allocations of aligned and misaligned movements in the second GLM would be the

consequence, leading to reduced or absent grid-cell-like representations. Statistically, spatial stability was evaluated with Rayleigh's test for non-uniformity of circular data (*46*), which was applied to the voxel-wise grid orientations of the first half of the data (accounting for spatial smoothing). This resulted in participant-wise z-values of spatial stability (for two examples, see Fig. 3C). In contrast, temporal instability means that the voxel-wise grid orientations – albeit potentially spatially stable – change across time. Incorrect allocations of aligned and misaligned movements in the second GLM would be the consequence, also producing reduced or absent grid-cell-like representations. To obtain a metric of temporal stability, we first calculated the voxel-wise grid orientations in the right EC ROI separately for both halves of the data. Afterwards, we evaluated for each voxel individually whether the grid orientation of the second half of the data was within a range of ± 15° around the grid orientation of the first half of the data. This allowed us to calculate the percentage of voxels with temporally stable grid orientations for each participant (for two examples, see Fig. 3A). For statistical comparison, percentage values ($\text{percentage}_{\text{original}}$) were logit-transformed according to: $\text{percentage}_{\text{new}} = \log[\text{percentage}_{\text{original}} / (1 - \text{percentage}_{\text{original}})]$, because they were in a limited range of 0 to 1 originally. For group statistics, temporal stability values (i.e. logit-transformed percentage values) and spatial stability values (i.e. Rayleigh's z-values) were entered into separate two-sample t-tests between genetic subgroups and into separate Pearson correlation analyses to detect significant relations to the grid-cell-like representations. Note that the terms "grid axes" and "grid orientation" used throughout the main paper and the Supplementary Information are based on a directionally modulated fMRI signal and do not simply correspond to electrophysiological nomenclature.

Functional connectivity between EC and hippocampus

Functional connectivity was analyzed by first extracting the preprocessed BOLD time series from right EC and right hippocampus and averaging them across voxels within each of the ROIs (right EC and right hippocampus). Next, linear trends of the time series were removed within sessions and the time series were normalized within sessions to have mean 0 and standard deviation 1. We calculated the Pearson correlation r value between the time series of right EC and right hippocampus for each participant and transformed the r values into z values (Fisher-z-transformation). As a control analysis, we included the participant-specific head motion parameters as regressors of no interest. As a second control analysis, functional connectivity between right EC and bilateral hippocampus as well as between right EC and left hippocampus was also calculated using the identical procedure.

Supplementary Text

Grid-cell-like representations and spatial memory performance within genetic subgroups

In the main text we showed that multiple regression was sensitive to reveal a positive relationship between the magnitude of grid-cell-like representations and spatial memory performance across all participants. To further evaluate a potential dependency of this relationship on genotype that would be relevant to proposing a mechanistic account of (later) spatial memory impairments observed in AD, we conducted two exploratory analyses. First, we plotted the raw bivariate correlations between grid-cell-like representations and spatial memory performance, separately for both genetic subgroups (Fig. S6A). Visual inspection suggests a stronger relationship in risk participants, but this was not significant (risk participants only: Pearson's $r = .204$, $P = .220$; control participants only: Pearson's $r = .055$, $P = .748$; difference between correlation coefficients, $z = .63$, $P = .529$). Second, we used partial correlations as a more sensitive approach correcting for sex, age, and central navigational preference, which revealed a significant partial correlation in risk participants ($r = .341$, $P = .045$; Fig. S6B), but not in control participants ($r = .086$, $P = .628$), with no difference between both groups ($z = 1.12$, $P = .263$). Thus, the most robust finding is an overall positive effect of grid-cell-like representations on spatial memory performance that is influenced by other factors such as sex, age, and central navigational preference as represented in the linear multiple regression analysis (Table 1).

Hippocampal task-related activity and spatial memory performance

To elucidate whether our finding of increased hippocampal task-related activity reflects compensatory mechanisms with a positive impact on behavior or adverse effects with a negative behavioral impact, we conducted two additional analyses (see Methods). First, different versions of the linear multiple regression (Table 1, including task-related activity of different parts of the hippocampus as an additional predictor, see Methods) showed that task-related activity of the entire hippocampus is too unspecific to reveal a positive association with spatial memory performance (bilateral, $P = .660$; left, $P = .465$; right, $P = .855$; Table S3, Models 1-3). However, activity in the posterior hippocampus (posterior third of the hippocampus), which seems to be more closely related to spatial navigation than the anterior hippocampus (*22*, *41-45*), was associated with improved spatial memory performance, in particular in the left hemisphere (bilateral, $P = .068$; left, $P = .006$; right, $P = .517$; Table S3, Models 4-6). This specificity was supported by our second-level whole brain analysis of voxels which are positively associated with spatial memory performance (within participants) and that are at the same time negatively associated with grid-cell-like representations (across participants; see Methods: "Confirmatory analysis of compensatory mechanisms"). This analysis revealed a brain-wide peak in the left posterior hippocampus (peak MNI coordinates: -18/-28/-8, peak z-score = 4.03, $P = .038$, FWE-corrected after small volume correction for the bilateral hippocampus; Fig. S9). Importantly, no other voxel exceeded this z-value on the whole brain level, reflecting the specificity of activation in the posterior hippocampus. Taken together, these two analyses suggest compensatory hippocampal task-related activity that is specific to its posterior third.

Interpretation of increased activity in *APOE*-ε4-carriers

It is a matter of ongoing debate whether increased hippocampal activity in *APOE*-ε4-carriers represents compensatory mechanisms required to maintain normal cognitive functioning or, in contrast, pathological dysfunction. Compensatory mechanisms in ε4-carriers were first suggested by Bookheimer et al. (*19*), similar to the finding of potential compensatory mechanisms in patients with mild AD (*47*) that could indeed be related to better performance (*48*). The hypothesis of compensatory mechanisms was further supported by findings of Bondi et al. (*49*), Rosano et al. (*50*), Han et al. (*51*), Filippini et al. (*21*), Wierenga et al. (*52*), and Suthana et al. (*53*). Even in a 20-year-old at risk for familial AD (presenilin 1 mutation carrier) increased brain activity within memory-related neural networks (including the hippocampus) was found and interpreted as compensatory effort (*54*). However, increased brain activity was also discussed as indicating different cognitive processing strategies, biochemical alterations, or as a marker of the pathophysiologic process itself (*55-57*). Moreover, there is growing evidence that hippocampal hyperactivity in mild cognitive impairment, AD, and presymptomatic individuals is a paradoxical or even adverse condition that could be targeted therapeutically (e.g., *58*, *59*). Jagust et al. (*60*) propose that lifespan brain activity in humans increases deposition of amyloid-β. Bakker et al. (*23*) even show that the reduction of hippocampal hyperactivity by the antiepileptic drug levetiracetam improves cognition in amnestic mild cognitive impairment. Furthermore, it is shown in mouse models that neuronal activity increases the regional load of amyloid-β deposition (*24*).

In the main text, we proposed that our finding of increased hippocampal activity indicates compensatory mechanisms in risk participants. This interpretation was based on our findings that reduced grid-cell-like representations were correlated with increased hippocampal task-related activity, and that this relationship was significantly more pronounced in risk participants as compared to control participants in the posterior hippocampus. In principle, there must be some compensatory processes given our contrary findings that spatial memory performance is preserved in risk participants, although they show reduced grid-cell-like representations and reduced central navigational preference, which are both related to impaired spatial memory performance across all participants. Increased hippocampal activity could reflect a more pronounced boundary-based navigation strategy in risk participants (*61*, *28*) or enhanced hippocampal path integration computations (*29*, *30*) to compensate for impaired entorhinal path integration. Furthermore, our finding that reduced grid-cell-like representations are also related to increased task-related activity in EC and amygdala (Fig. S8) could be interpreted as an overall compensatory activity of the medial temporal lobe areas. For example, Filippini et al. (*21*) speculate that increased activity in hippocampal regions reflects compensation of reduced synaptic plasticity, neuronal growth, or altered long-term potentiation, which seems to be particularly affected by apolipoprotein E4 (*62*). However, this finding could also speak in favor of an adverse broader disruption of medial lobe network computations accounting in total for our finding of altered navigational behavior in risk participants. Hence, to further elucidate whether our finding of increased hippocampal task-related activity could represent compensatory mechanisms with a behavioral impact, we conducted two additional analyses (see Supplementary Text

"Hippocampal task-related activity and spatial memory performance"). It became apparent that increased task-related activity specifically of the (left) posterior hippocampus is related to better behavioral performance, supporting the compensatory hypothesis. Furthermore, our finding of reduced functional connectivity between EC and hippocampus in participants with reduced temporal stability values (Fig. S10B) might reflect a mechanism to protect hippocampal processing from impaired entorhinal computations enabling independent compensatory mechanisms. However, the last two results were obtained across all participants and were not modulated by genotype (no differences between correlation coefficients were observed). While this speaks against a compensatory role that is specific to risk participants, it is consistent with the general idea that entorhinal cortex dysfunction is associated with (and possibly responsible for) broader changes in medial temporal lobe computations. In this light, *APOE*-ε4 may induce entorhinal dysfunction that could then, in turn, gradually lead to functional changes in downstream areas. Finally, we would like to point out that the two interpretations of increased hippocampal activity as a compensatory or a pathological phenomenon are not mutually exclusive: increased hippocampal activity could (temporarily) serve as a compensatory mechanism – in particular in young participants, decades before potential disease onset – and simultaneously promote pathological processes. The compensatory potential might then fade out with proceeding pathology or might be shifted to neocortical areas as suggested in various studies (e.g., *53*).

Functional connectivity between right EC and hippocampus

We found that there was pronounced functional connectivity between right EC and right hippocampus across all participants (one-sample *t*-test, $t_{74} = 36.561$, $P < .001$). Furthermore, reduced temporal stability values were associated with lower connectivity values (Pearson's $r = .298$, $P = .009$; Fig. S10B), possibly indicating a decoupling of both regions associated with entorhinal dysfunction. This decoupling between right EC and right hippocampus could constitute a modulating mechanism to reduce the influence of impaired entorhinal computations on hippocampal processing. Independent hippocampal functioning may thus be enabled that could compensate for EC failure. For completeness, similar results were achieved when using the time series from right EC and bilateral hippocampus (correlation to temporal stability values: Pearson's $r = .272$, $P = .018$) or right EC and left hippocampus (correlation to temporal stability values: Pearson's $r = .229$, $P = .048$). Likewise, including the participant-specific head motion parameters (as potential confounds of functional connectivity) did not change the results substantially (correlation between temporal stability values and functional connectivity between right EC and right hippocampus, Pearson's $r = .282$, $P = .014$).

Potential mechanistic basis of reduced grid-cell-like representations in risk participants

We speculate that risk participants exhibit less robust grid-cell-like representations and temporally unstable grid orientations in combination with preserved spatial stability of the grid orientations because of the underlying neuropathological changes: Intraneuronal neurofibrillary tangles – potentially impairing grid cell inherent properties such as temporal stability and strength of the grid representations – and not interneuronal amyloid-β plaques – possibly affecting synaptic communication between grid cells and thus spatial stability of the grid orientations – appear first in

histopathological sections, especially in *APOE*-ε4-carriers (*6*, *7*). These hypotheses could be tested in mouse models of AD.

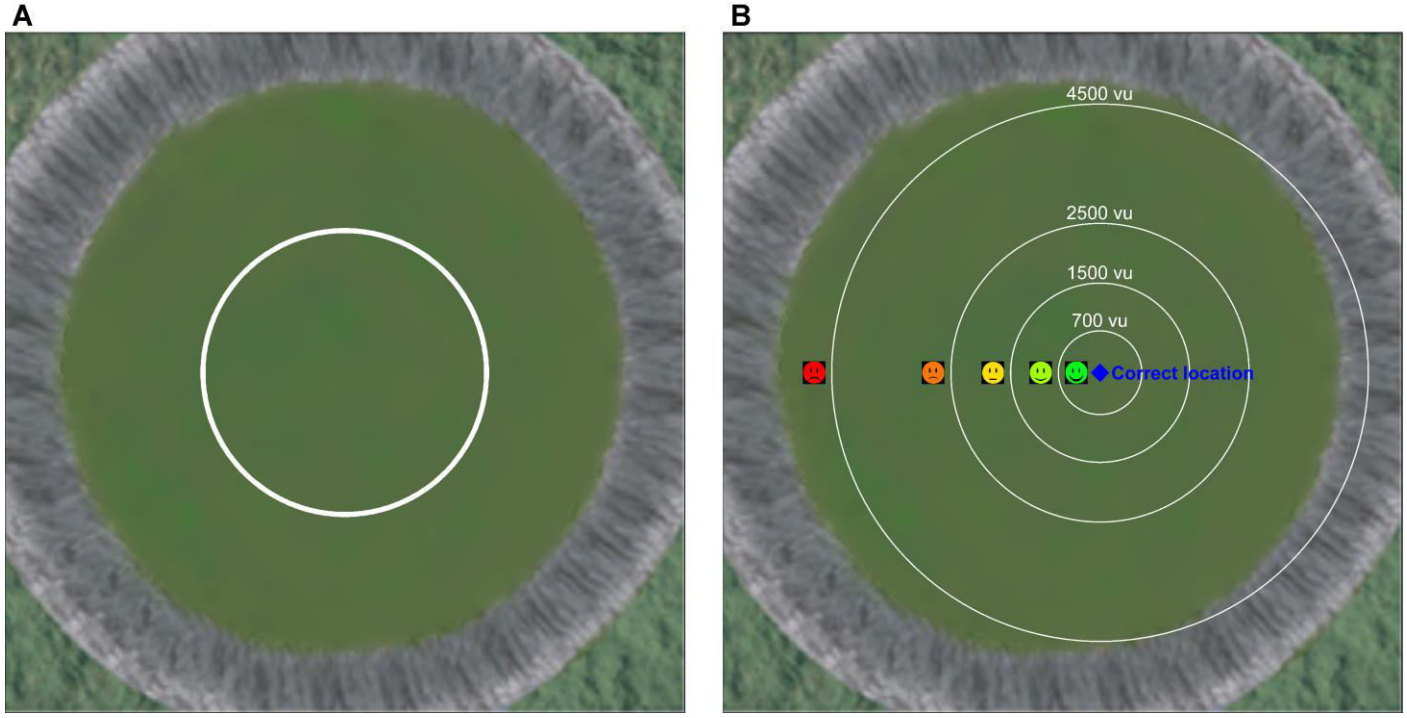

Fig. S1. Illustration of central navigational preference and feedback. (**A**) Participant-specific values of central navigational preference were calculated as central navigational preference = n_{center} / $n_{periphery}$, where n_{center} is the number of time points spent in the center of the arena (within circle) and $n_{periphery}$ is the number of time points spent in the periphery of the arena (outside circle). The division into center and periphery was drawn by dividing the arena radius into two equal halves. Solely time points during the retrieval phase were considered, as we expected a behavioral relevance for correct object placement only during this trial phase. (**B**) After placement of the object, participants received feedback via one of five smiley faces. E.g., dark green smiley faces were shown when the participant placed the object within a radius of 700 virtual units (vu) around the correct object location.

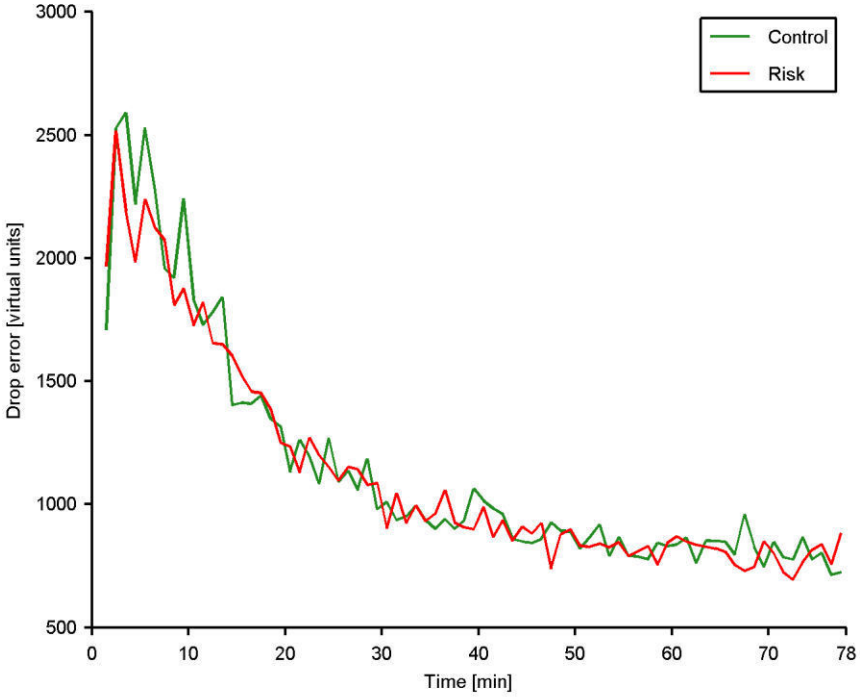

Fig. S2. Learning curves. Participants gradually improved their performance throughout the experiment. As expected, drop errors decreased with time. However, they did not vary as a function of genotype or time-genotype-interaction (time × genotype repeated measures ANOVA: main effect of time, $F_{76,5548} = 32.326$, $P < .001$; no main effect of genotype, $F_{1,73} = .031$, $P = .860$; no interaction, $F_{76,5548} = .643$, $P = .993$).

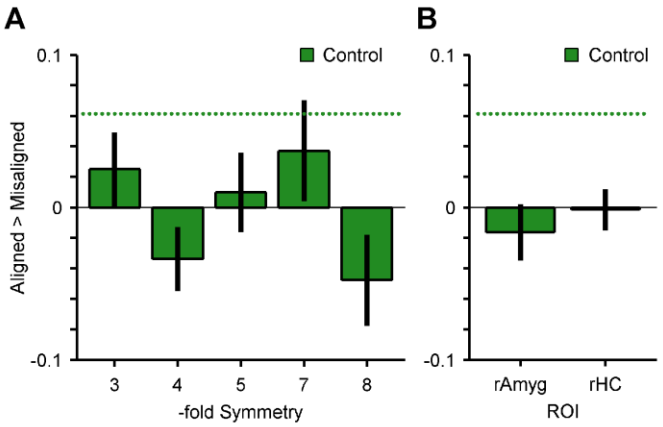

Fig. S3. Control analyses. (**A**) Absence of "Aligned > Misaligned" effects in 3-, 4-, 5-, 7-, and 8-fold rotational symmetry control models for control participants (all $P > .112$). (**B**) 6-fold rotational symmetry in right amygdala ("rAmyg") or right hippocampus ("rHC") does not lead to consistent grid-cell-like representations ("Aligned > Misaligned") in control participants (both $P > .382$). These results show that our finding in control participants is specific for six-fold rotational symmetry and specific for right EC. Green dotted line represents the result of 6-fold rotational symmetry in the right EC of control participants from Fig. 2B. All bars show mean and SEM across participants. Units of all contrasts are parameter estimates.

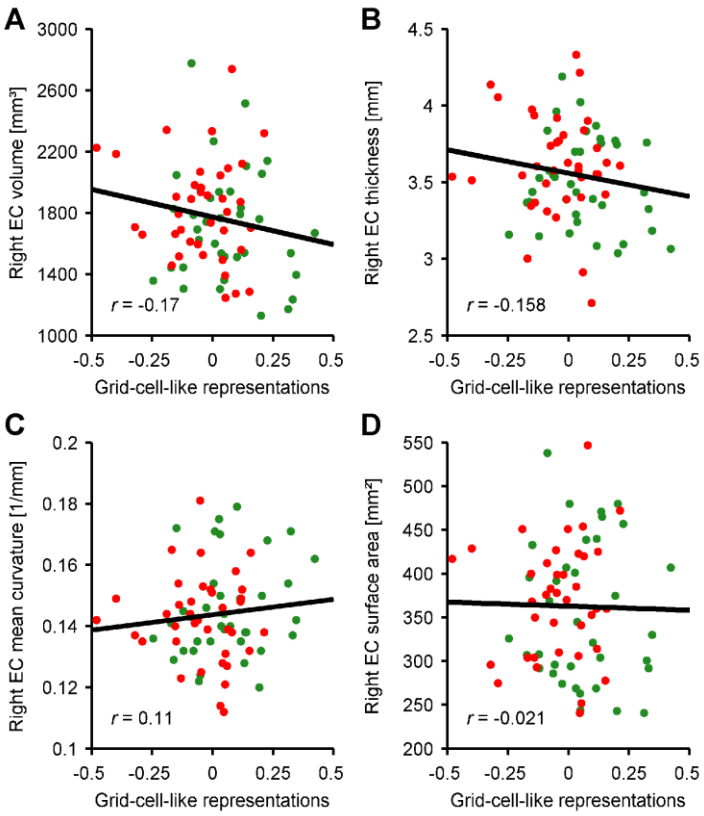

Fig. S4. Grid-cell-like representations and participant-wise structural metrics of the right entorhinal cortex. Pearson correlations did not reveal associations between grid-cell-like representations and right EC structural metrics across participants, which could potentially account for the functional changes: (**A**) volume, $P = .145$, (**B**) thickness, $P = .177$, (**C**) mean curvature, $P = .348$, (**D**) surface area, $P = .861$. Correlation coefficients did not differ between genetic subgroups. Structural metrics were obtained using the Freesurfer image analysis suite (see Methods). Green dots represent control participants, red dots represent risk participants. Units of grid-cell-like representations are parameter estimates.

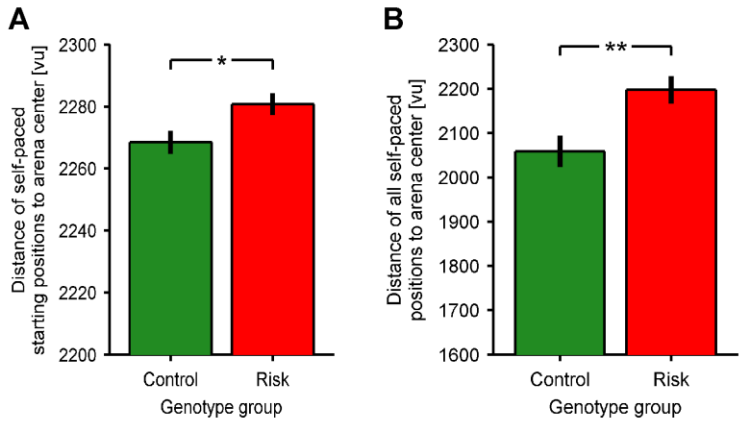

Fig. S5. Absolute distances of the self-paced positions relative to the arena center in the virtual environment. In accordance with our finding of reduced central navigational preference, risk participants exhibited greater mean distances of the (**A**) self-paced starting positions (at the beginning of each retrieval phase, except for the very first retrieval phase) as well as greater mean distances of (**B**) all self-paced positions (during all cue, retrieval, feedback, and re-encoding phases) relative to the arena center of the virtual environment. All bars show mean and SEM across participants. *$P < .05$, **$P < .01$.

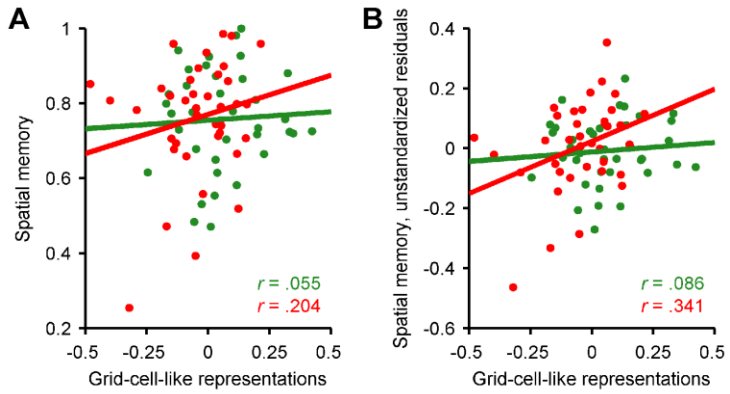

Fig. S6. Grid-cell-like representations and spatial memory performance within genetic subgroups. (**A**) Raw bivariate Pearson correlations between grid-cell-like representations and spatial memory performance. Risk participants only: $P = .220$; control participants only: $P = .748$; difference between correlation coefficients: $z = .63$, $P = .529$. (**B**) Partial correlations between grid-cell-like representations and spatial memory performance correcting for sex, age, and central navigational preference, separately for both genetic subgroups. Risk participants only: $P = .045$; control participants only: $P = .628$; difference between correlation coefficients: $z = 1.12$, $P = .263$. Green dots represent control participants, red dots represent risk participants. Units of grid-cell-like representations are parameter estimates.

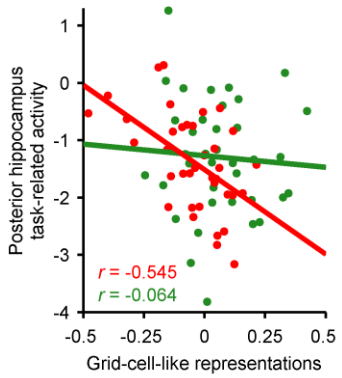

Fig. S7. Genotype dependent relation between task-related activity in the posterior hippocampus and magnitude of grid-cell-like representations. In the posterior hippocampus, the negative correlation between task-related hippocampal activity and the magnitude of grid-cell-like representations is significantly different between genetic subgroups ($P = .023$): Whereas risk participants show a highly significant correlation ($P < .001$), this effect is not present in control participants ($P = .707$). Green dots represent control participants, red dots represent risk participants. Units of grid-cell-like representations and task-related activity are parameter estimates.

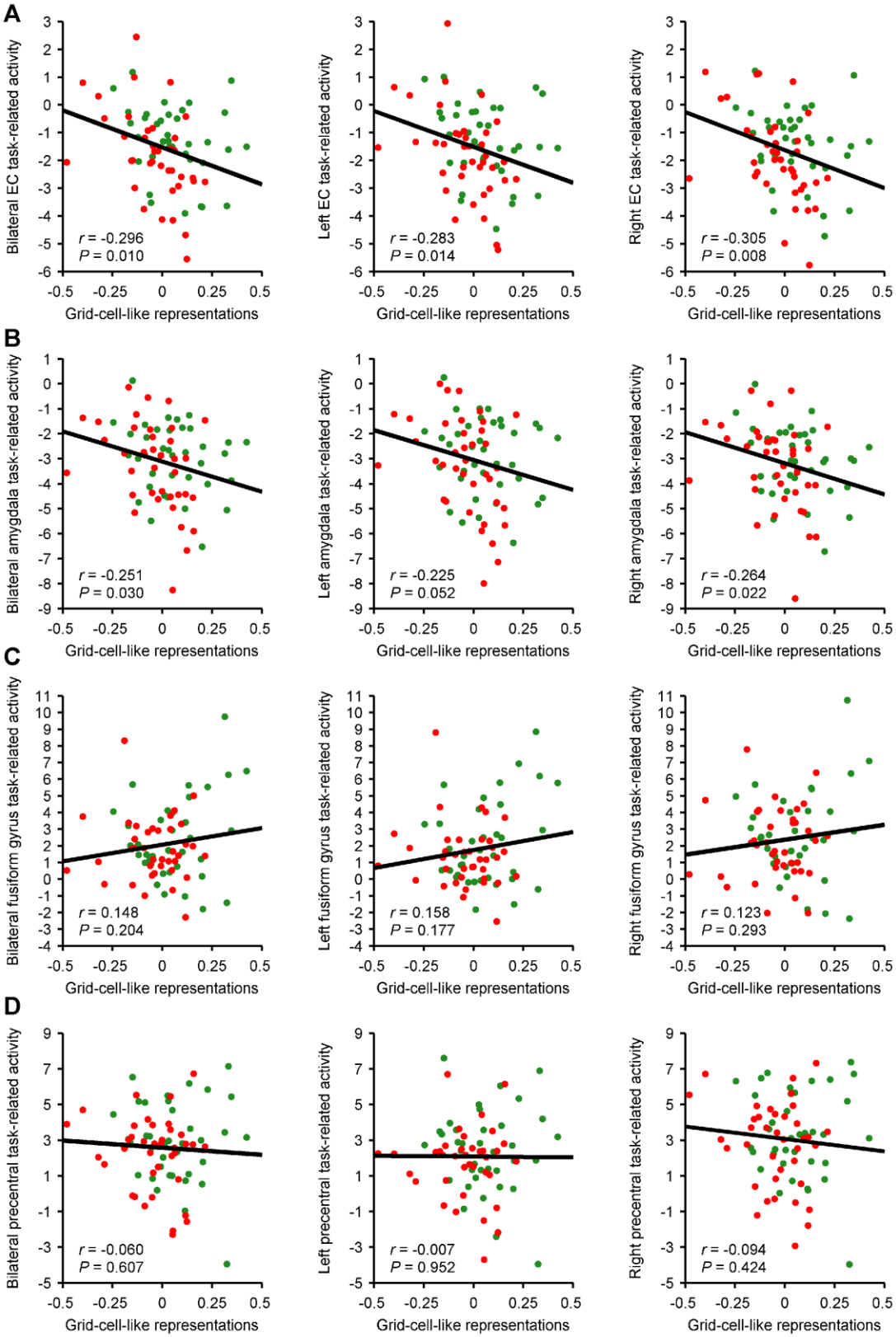

Fig. S8. Grid-cell-like representations and task-related activity. Reduced grid-cell-

like representations were not only related to increased task-related activity in the hippocampus (Fig. 2C), but also to increased task-related activity in EC (**A**) and amygdala (**B**). Fusiform gyrus (**C**) and the precentral cortex (**D**) were chosen as control regions outside the medial temporal lobe. *P*- and *r*-values refer to Pearson correlations. Correlation coefficients did not differ between genetic subgroups. In sum, these data suggest that reduced grid-cell-like representations are related to an overall increase in medial temporal lobe activity. Green dots represent control participants, red dots represent risk participants. Plots on the left show bilateral regions, plots in the middle refer to regions in the left hemisphere, and plots on the right display effects in the right hemisphere. Units of grid-cell-like representations and task-related activity are parameter estimates.

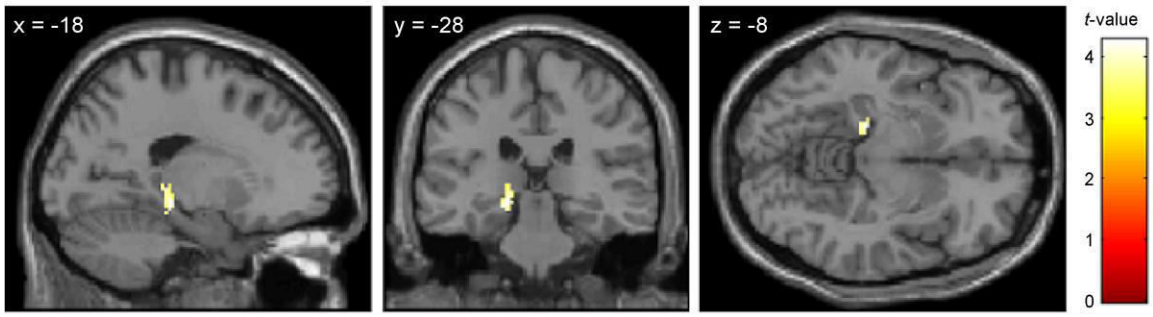

Fig. S9. Confirmatory analysis of compensatory hippocampal activity. Grid-cell-like representations correlated negatively with activity in left posterior hippocampus that was enhanced during trials with more accurate object placement (peak MNI coordinates: -18/-28/-8, peak *z*-score = 4.03, $P = .038$, FWE-corrected after small volume correction for bilateral hippocampus, *t*-image thresholded at $P < .0005$, and voxel extent = 10 for display purposes). No other voxel exceeded this *z*-value on whole brain level. Color bar indicates *t*-statistics. This result supports our previous ROI-result of compensatory hippocampal task-related activity.

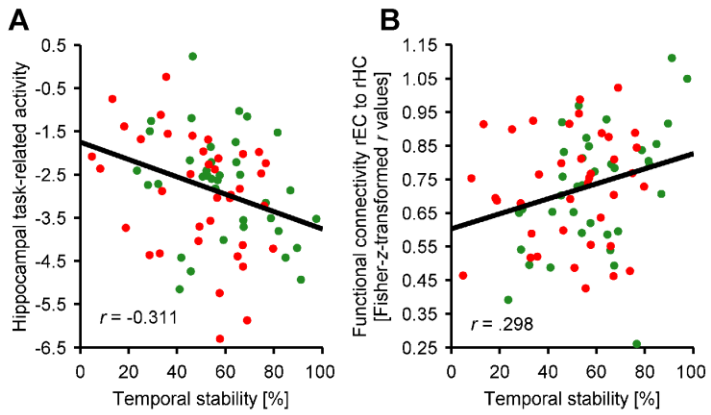

Fig. S10. Temporal stability of voxel-wise grid orientations. (**A**) Higher temporal stability values are significantly correlated with lower hippocampal task-related activity (Pearson correlation, $P = .007$). (**B**) Reduced temporal stability values are related to decreased functional connectivity between right EC and right hippocampus (Pearson correlation, $P = .009$). rEC, right entorhinal cortex; rHC, right hippocampus. Green dots represent control participants, red dots represent risk participants.

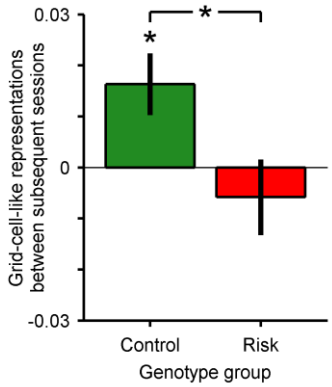

Fig. S11. Grid-cell-like representations under the condition of similar stability values between genetic subgroups. Performing the analysis of grid-cell-like representations on shorter data segments (within subsequent pairs of sessions, see Methods) reveals significant right EC grid-cell-like representations in control participants (one-sample *t*-test, $t_{36} = 2.708$, $P = .010$) but not in risk participants (one-sample *t*-test, $t_{37} = -.788$, $P = .436$), with a significant difference between both groups (two-sample *t*-test, $t_{73} = 2.315$, $P = .023$). In contrast, temporal and spatial stability values do not differ between groups. Bars show mean and SEM across participants. Units of grid-cell-like representations are parameter estimates. *$P < .05$.

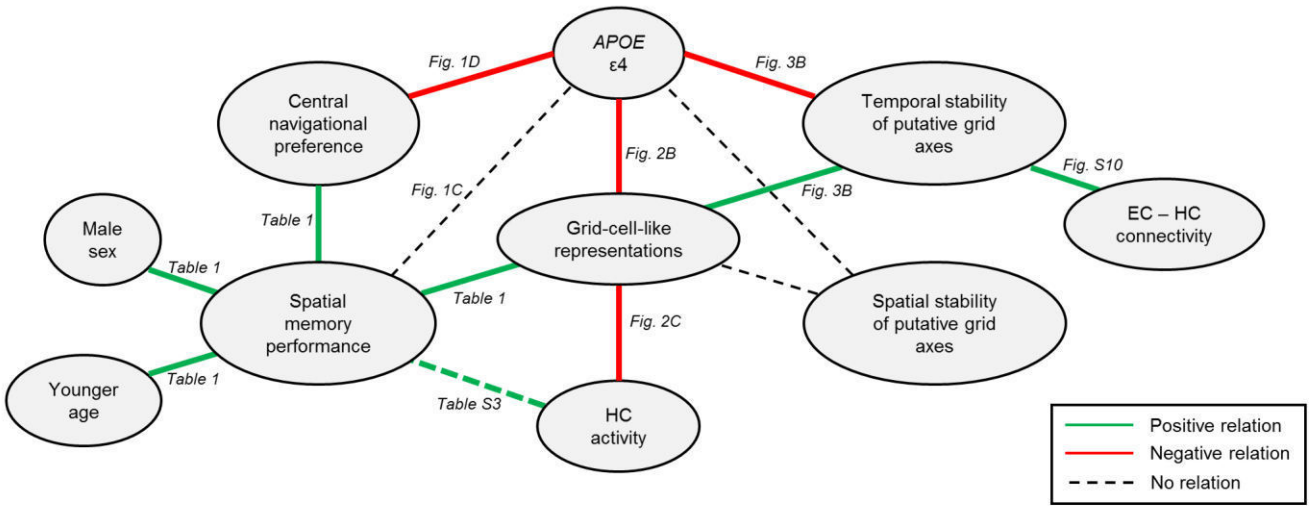

Fig. S12. Schematic overview of all results. EC, right entorhinal cortex; HC, hippocampus. Dashed green line indicates a positive relation between spatial memory performance and HC activity that is specific to the left posterior third of the hippocampus (see Table S3).

Table S1. Demographic characteristics of participants.

	Control group (*APOE* ε3, ε3)	**Risk group (*APOE* ε4, ε3)**	***P***
Number	37	38	
Mean age, age range [years]	22.76 (± .49), 18-30	22.34 (± .45), 18-29	.532[a]
Sex [male/ female]	18/ 19	18/ 20	.912[c]
Education [years]	16.19 (± .38)	16.05 (± .37)	.693[b]
Family history of dementia	2	3	.667[c]

Values denote mean (± SEM) or the number of participants. *P*-values refer to [(a)] two-sample *t*-tests, [(b)] Mann-Whitney *U* tests, or [(c)] χ^2-tests.

Table S2. Influence of *APOE* genotype on basic behavioral characteristics.

	Control group (*APOE* ε3, ε3)	**Risk group (*APOE* ε4, ε3)**	***P***
Number of movement time points [10/s]	19,937 (± 422)	19,967 (± 441)	.961[a]
Cut-off speed [vu/s]	799 (± 1)	799 (± 1)	.611[b]
Total path length [vu]	1,451,250 (± 45,626)	1,447,604 (± 48,265)	.956[a]
Number of trials	229 (± 8.8)	230 (± 6.7)	.918[a]
Duration of retrieval-phases [s]	11.8 (± .7)	11.1 (± .5)	.453[a]
Duration of re-encoding-phases [s]	5.4 (± .3)	5.1 (± .2)	.679[b]

Values denote mean (± SEM). *P*-values refer to [(a)] two-sample *t*-tests or [(b)] Mann-Whitney *U* tests. s, seconds; vu, virtual units.

Table S3. Multiple regression to predict spatial memory performance including task-related activity of different parts of the hippocampus (*N* = 75).

Predictor	β	*t*	*P*
Model 1: including task-related activity in bilateral hippocampus (adjusted R^2 = .161; all VIF < 1.441)			
Grid-cell-like representations	.256	2.093	.040*
Central navigational preference	.235	2.106	.039*
Genotype [control/ risk]	.146	1.230	.223
Sex [male/ female]	-.258	-2.149	.035*
Age [years]	-.304	-2.795	.007**
Task-related activity (bilateral hippocampus)	.057	.442	.660
Model 2: including task-related activity in left hippocampus (adjusted R^2 = .165; all VIF < 1.471)			
Grid-cell-like representations	.270	2.196	.032*
Central navigational preference	.232	2.080	.041*
Genotype [control/ risk]	.154	1.292	.201
Sex [male/ female]	-.242	-2.017	.048*
Age [years]	-.306	-2.826	.006**
Task-related activity (left hippocampus)	.095	.735	.465
Model 3: including task-related activity in right hippocampus (adjusted R^2 = .159; all VIF < 1.347)			
Grid-cell-like representations	.230	1.904	.061(*)
Central navigational preference	.236	2.115	.038*
Genotype [control/ risk]	.134	1.120	.267
Sex [male/ female]	-.290	-2.479	.016*
Age [years]	-.307	-2.816	.006**
Task-related activity (right hippocampus)	-.023	-.183	.855
Model 4: including task-related activity in bilateral posterior hippocampus (adjusted R^2 = .199; all VIF < 1.359)			
Grid-cell-like representations	.278	2.433	.018*
Central navigational preference	.234	2.146	.035*
Genotype [control/ risk]	.167	1.440	.155

Sex [male/ female]	-.178	-1.504	.137
Age [years]	-.311	-2.923	.005**
Task-related activity (bilateral posterior hippocampus)	.225	1.856	.068$^{(*)}$
Model 5: including task-related activity in left posterior hippocampus (adjusted R^2 = .248; all VIF < 1.356)			
Grid-cell-like representations	.286	2.597	.012*
Central navigational preference	.238	2.260	.027*
Genotype [control/ risk]	.173	1.546	.127
Sex [male/ female]	-.123	-1.058	.294
Age [years]	-.308	-2.993	.004**
Task-related activity (left posterior hippocampus)	.334	2.848	.006**
Model 6: including task-related activity in right posterior hippocampus (adjusted R^2 = .163; all VIF < 1.265)			
Grid-cell-like representations	.254	2.160	.034*
Central navigational preference	.235	2.109	.039*
Genotype [control/ risk]	.148	1.253	.214
Sex [male/ female]	-.252	-2.163	.034*
Age [years]	-.307	-2.826	.006**
Task-related activity (right posterior hippocampus)	.078	.651	.517

Multicollinearity was not a concern (see variance inflation factors, VIF). $^{(*)}P < .10$, $*P < .05$, $**P < .010$.

Table S4. Detailed description of the first general linear model (GLM) to identify the angular orientation of the putative grid axes relative to the environment in each participant's right EC. For this general linear model (GLM) one half of the data was used (sessions 1, 3, and 5). All regressors were convolved with the canonical hemodynamic response function (HRF) in SPM before entering the GLM. Data were high-pass filtered at 1/128 Hz. Coefficients for each regressor were estimated for each participant using maximum likelihood estimates.

Regressor	Parametric modulator	Temporal derivative modeled	Duration [seconds]
Regressors to analyze grid-cell-like representations			
Movement		Yes	0
	$\sin[\alpha(t) * 6]$[a]	Yes	0
	$\cos[\alpha(t) * 6]$[a]	Yes	0
Regressors to model trial phases			
Cue	-	Yes	0
Retrieval	-	Yes	Variable
Feedback	-	Yes	0
Re-encoding	-	Yes	Variable
Nuisance regressors			
Scanner drift	-	No	Session[b]
Mean activation	-	No	Session
Head motion parameters	-	No	Session

[(a)] $\alpha(t)$ is angular movement direction at time point t. [(b)] The duration of one session is 13 min.

Table S5. Second GLM to contrast brain activity during aligned movements with brain activity during misaligned movements relative to the previously identified grid axes. For this GLM the other half of the data was used (sessions 2, 4, and 6). All regressors were convolved with the canonical HRF in SPM before entering the GLM. Data were high-pass filtered at 1/128 Hz. Coefficients for each regressor were estimated for each participant using maximum likelihood estimates. The estimated contrast values of aligned versus misaligned movements are termed "grid-cell-like representations".

Regressor	Temporal derivative modeled	Duration [seconds]
Regressors to analyze grid-cell-like representations		
Aligned movement	Yes	0
Misaligned movement	Yes	0
Regressors to model trial phases		
Cue	Yes	0
Retrieval	Yes	Variable
Feedback	Yes	0
Re-encoding	Yes	Variable
Nuisance regressors		
Scanner drift	No	Session
Mean activation	No	Session
Head motion parameters	No	Session

Table S6. GLM to estimate hippocampal task-related activity. All regressors were convolved with the canonical hemodynamic response function (HRF) in SPM before entering the GLM. Data were high-pass filtered at 1/128 Hz. Coefficients for each regressor were estimated for each participant using maximum likelihood estimates.

Regressor	**Temporal derivative modeled**	**Duration [seconds]**
Regressor to model hippocampal task-related activation		
Cue + retrieval + feedback + re-encoding	Yes	Variable
Nuisance regressors		
Scanner drift	No	Session
Mean activation	No	Session
Head motion parameters	No	Session

Table S7. GLM for the confirmatory analysis of compensatory hippocampal activity. The aim of this GLM was to reveal voxel activity associated with spatial memory performance. Hence, we modeled the retrieval phase with a parametric modulator, termed "Response accuracy", which was determined as follows. For each participant separately, the 20%-, 40%-, 60%-, 80%-, and 100%-quantile of all drop errors were calculated. Note that the drop error was defined as the distance between the response location and the correct location (thus having a reverse relation to spatial memory performance). Next, we assigned the highest value of +2 to the parametric modulator, when the trial-specific drop error was in the lowest quantile of all drop errors, the value of +1, when the trial-specific drop error was in the second lowest quantile of all drop errors, and the values 0, -1, and -2, when the trial-specific drop errors were in the middle, second highest, and highest quantile, respectively. All regressors were convolved with the canonical HRF in SPM before entering the GLM. Data were high-pass filtered at 1/128 Hz. Coefficients for each regressor were estimated for each participant using maximum likelihood estimates. Contrast values for the parametric modulator versus zero across all sessions were calculated for all participants and entered into a second level random effects linear regression analysis as implemented in SPM. During the second level analysis, we were then able to look for spatial memory-related brain activations negatively correlated to grid-cell-like representations, also reflecting compensatory activations.

Regressor	Parametric modulator	Temporal derivative modeled	Duration [seconds]
Regressors to model trial phases and response accuracy			
Cue	-	Yes	0
Retrieval		Yes	Variable
	Response accuracy[a]	Yes	Variable
Feedback	-	Yes	0
Re-encoding	-	Yes	Variable
Nuisance regressors			
Scanner drift	-	No	Session
Mean activation	-	No	Session
Head motion parameters	-	No	Session

[(a)] The parametric modulator contained equally distributed values of +2, +1, 0, -1, and -2.

REFERENCES

1. H. W. Querfurth, F. M. LaFerla, Alzheimer's disease. *N. Engl. J. Med.* **362**, 329–344 (2010). Medline doi:10.1056/NEJMra0909142

2. R. A. Sperling, C. R. Jack Jr., P. S. Aisen, Testing the right target and right drug at the right stage. *Sci. Transl. Med.* **3**, 111cm33 (2011). Medline

3. E. H. Corder, A. M. Saunders, W. J. Strittmatter, D. E. Schmechel, P. C. Gaskell, G. W. Small, A. D. Roses, J. L. Haines, M. A. Pericak-Vance, Gene dose of apolipoprotein E type 4 allele and the risk of Alzheimer's disease in late onset families. *Science* **261**, 921–923 (1993). Medline doi:10.1126/science.8346443

4. C. C. Liu, T. Kanekiyo, H. Xu, G. Bu, Apolipoprotein E and Alzheimer disease: Risk, mechanisms and therapy. *Nat. Rev. Neurol.* **9**, 106–118 (2013). Medline doi:10.1038/nrneurol.2012.263

5. H. Braak, E. Braak, Neuropathological stageing of Alzheimer-related changes. *Acta Neuropathol.* **82**, 239–259 (1991). Medline doi:10.1007/BF00308809

6. H. Braak, K. Del Tredici, The pathological process underlying Alzheimer's disease in individuals under thirty. *Acta Neuropathol.* **121**, 171–181 (2011). Medline doi:10.1007/s00401-010-0789-4

7. E. Ghebremedhin, C. Schultz, E. Braak, H. Braak, High frequency of apolipoprotein E ε4 allele in young individuals with very mild Alzheimer's disease-related neurofibrillary changes. *Exp. Neurol.* **153**, 152–155 (1998). Medline doi:10.1006/exnr.1998.6860

8. T. Hafting, M. Fyhn, S. Molden, M. B. Moser, E. I. Moser, Microstructure of a spatial map in the entorhinal cortex. *Nature* **436**, 801–806 (2005). Medline doi:10.1038/nature03721

9. J. Jacobs, C. T. Weidemann, J. F. Miller, A. Solway, J. F. Burke, X. X. Wei, N. Suthana, M. R. Sperling, A. D. Sharan, I. Fried, M. J. Kahana, Direct recordings of grid-like neuronal activity in human spatial navigation. *Nat. Neurosci.* **16**, 1188–1190 (2013). Medline doi:10.1038/nn.3466

10. G. Buzsáki, E. I. Moser, Memory, navigation and theta rhythm in the hippocampal-entorhinal system. *Nat. Neurosci.* **16**, 130–138 (2013). Medline doi:10.1038/nn.3304

11. M. E. Hasselmo, M. P. Brandon, Linking cellular mechanisms to behavior: Entorhinal persistent spiking and membrane potential oscillations may underlie path integration, grid cell firing, and episodic memory. *Neural Plast.* **2008**, 658323 (2008). Medline doi:10.1155/2008/658323

12. S. Sreenivasan, I. Fiete, Grid cells generate an analog error-correcting code for singularly precise neural computation. *Nat. Neurosci.* **14**, 1330–1337 (2011). Medline doi:10.1038/nn.2901

13. D. Bush, C. Barry, N. Burgess, What do grid cells contribute to place cell firing? *Trends Neurosci.* **37**, 136–145 (2014). Medline doi:10.1016/j.tins.2013.12.003

14. A. D. Ekstrom, M. J. Kahana, J. B. Caplan, T. A. Fields, E. A. Isham, E. L. Newman, I. Fried, Cellular networks underlying human spatial navigation. *Nature* **425**, 184–188 (2003). Medline doi:10.1038/nature01964

15. C. F. Doeller, C. Barry, N. Burgess, Evidence for grid cells in a human memory network. *Nature* **463**, 657–661 (2010). Medline doi:10.1038/nature08704

16. Materials and methods are available as supplementary materials on *Science* Online.

17. F. Berteau-Pavy, B. Park, J. Raber, Effects of sex and *APOE* ε4 on object recognition and spatial navigation in the elderly. *Neuroscience* **147**, 6–17 (2007). Medline doi:10.1016/j.neuroscience.2007.03.005

18. M. J. Chadwick, A. E. Jolly, D. P. Amos, D. Hassabis, H. J. Spiers, A goal direction signal in the human entorhinal/subicular region. *Curr. Biol.* **25**, 87–92 (2015). Medline doi:10.1016/j.cub.2014.11.001

19. S. Y. Bookheimer, M. H. Strojwas, M. S. Cohen, A. M. Saunders, M. A. Pericak-Vance, J. C. Mazziotta, G. W. Small, Patterns of brain activation in people at risk for Alzheimer's disease. *N. Engl. J. Med.* **343**, 450–456 (2000). Medline doi:10.1056/NEJM200008173430701

20. B. A. Strange, M. P. Witter, E. S. Lein, E. I. Moser, Functional organization of the hippocampal longitudinal axis. *Nat. Rev. Neurosci.* **15**, 655–669 (2014). Medline doi:10.1038/nrn3785

21. N. Filippini, B. J. MacIntosh, M. G. Hough, G. M. Goodwin, G. B. Frisoni, S. M. Smith, P. M. Matthews, C. F. Beckmann, C. E. Mackay, Distinct patterns of brain activity in young carriers of the *APOE*-ε4 allele. *Proc. Natl. Acad. Sci. U.S.A.* **106**, 7209–7214 (2009). Medline doi:10.1073/pnas.0811879106

22. M. S. Fanselow, H. W. Dong, Are the dorsal and ventral hippocampus functionally distinct structures? *Neuron* **65**, 7–19 (2010). Medline doi:10.1016/j.neuron.2009.11.031

23. A. Bakker, G. L. Krauss, M. S. Albert, C. L. Speck, L. R. Jones, C. E. Stark, M. A. Yassa, S. S. Bassett, A. L. Shelton, M. Gallagher, Reduction of hippocampal hyperactivity improves cognition in amnestic mild cognitive impairment. *Neuron* **74**, 467–474 (2012). Medline doi:10.1016/j.neuron.2012.03.023

24. A. W. Bero, P. Yan, J. H. Roh, J. R. Cirrito, F. R. Stewart, M. E. Raichle, J. M. Lee, D. M. Holtzman, Neuronal activity regulates the regional vulnerability to amyloid-β deposition. *Nat. Neurosci.* **14**, 750–756 (2011). Medline doi:10.1038/nn.2801

25. K. Hardcastle, S. Ganguli, L. M. Giocomo, Environmental boundaries as an error correction mechanism for grid cells. *Neuron* **86**, 827–839 (2015). Medline doi:10.1016/j.neuron.2015.03.039

26. L. Muessig, J. Hauser, T. J. Wills, F. Cacucci, A developmental switch in place cell accuracy coincides with grid cell maturation. *Neuron* **86**, 1167–1173 (2015). Medline doi:10.1016/j.neuron.2015.05.011

27. A. J. Trachtenberg, N. Filippini, C. E. Mackay, The effects of APOE-ε4 on the BOLD response. *Neurobiol. Aging* **33**, 323–334 (2012). Medline doi:10.1016/j.neurobiolaging.2010.03.009

28. C. F. Doeller, J. A. King, N. Burgess, Parallel striatal and hippocampal systems for landmarks and boundaries in spatial memory. *Proc. Natl. Acad. Sci. U.S.A.* **105**, 5915–5920 (2008). Medline doi:10.1073/pnas.0801489105

29. T. Wolbers, J. M. Wiener, H. A. Mallot, C. Büchel, Differential recruitment of the hippocampus, medial prefrontal cortex, and the human motion complex during path integration in humans. *J. Neurosci.* **27**, 9408–9416 (2007). Medline doi:10.1523/JNEUROSCI.2146-07.2007

30. K. R. Sherrill, U. M. Erdem, R. S. Ross, T. I. Brown, M. E. Hasselmo, C. E. Stern, Hippocampus and retrosplenial cortex combine path integration signals for successful navigation. *J. Neurosci.* **33**, 19304–19313 (2013). Medline doi:10.1523/JNEUROSCI.1825-13.2013

31. C. R. Mondadori, D. J. de Quervain, A. Buchmann, H. Mustovic, M. A. Wollmer, C. F. Schmidt, P. Boesiger, C. Hock, R. M. Nitsch, A. Papassotiropoulos, K. Henke, Better memory and neural efficiency in young apolipoprotein E ε4 carriers. *Cereb. Cortex* **17**, 1934–1947 (2007). Medline doi:10.1093/cercor/bhl103

32. F. Cacucci, M. Yi, T. J. Wills, P. Chapman, J. O'Keefe, Place cell firing correlates with memory deficits and amyloid plaque burden in Tg2576 Alzheimer mouse model. *Proc. Natl. Acad. Sci. U.S.A.* **105**, 7863–7868 (2008). Medline doi:10.1073/pnas.0802908105

33. T. Stöcker, T. Kellermann, F. Schneider, U. Habel, K. Amunts, P. Pieperhoff, K. Zilles, N. J. Shah, Dependence of amygdala activation on echo time: Results from olfactory fMRI experiments. *Neuroimage* **30**, 151–159 (2006). Medline doi:10.1016/j.neuroimage.2005.09.050

34. J. Ashburner, K. J. Friston, Unified segmentation. *Neuroimage* **26**, 839–851 (2005). Medline doi:10.1016/j.neuroimage.2005.02.018

35. A. M. Dale, B. Fischl, M. I. Sereno, Cortical surface-based analysis. I. Segmentation and surface reconstruction. *Neuroimage* **9**, 179–194 (1999). Medline doi:10.1006/nimg.1998.0395

36. B. Fischl, M. I. Sereno, A. M. Dale, Cortical surface-based analysis. II: Inflation, flattening, and a surface-based coordinate system. *Neuroimage* **9**, 195–207 (1999). Medline doi:10.1006/nimg.1998.0396

37. B. Fischl, A. M. Dale, Measuring the thickness of the human cerebral cortex from magnetic resonance images. *Proc. Natl. Acad. Sci. U.S.A.* **97**, 11050–11055 (2000). Medline doi:10.1073/pnas.200033797

38. B. Fischl, D. H. Salat, E. Busa, M. Albert, M. Dieterich, C. Haselgrove, A. van der Kouwe, R. Killiany, D. Kennedy, S. Klaveness, A. Montillo, N. Makris, B. Rosen, A. M. Dale, Whole brain segmentation: Automated labeling of neuroanatomical structures in the human brain. *Neuron* **33**, 341–355 (2002). Medline doi:10.1016/S0896-6273(02)00569-X

39. R. Insausti, K. Juottonen, H. Soininen, A. M. Insausti, K. Partanen, P. Vainio, M. P. Laakso, A. Pitkänen, MR volumetric analysis of the human entorhinal, perirhinal, and temporopolar cortices. *Am. J. Neuroradiol.* **19**, 659–671 (1998). Medline

40. C. Watson, F. Andermann, P. Gloor, M. Jones-Gotman, T. Peters, A. Evans, A. Olivier, D. Melanson, G. Leroux, Anatomic basis of amygdaloid and hippocampal volume measurement by magnetic resonance imaging. *Neurology* **42**, 1743–1750 (1992). Medline doi:10.1212/WNL.42.9.1743

41. E. A. Maguire, D. G. Gadian, I. S. Johnsrude, C. D. Good, J. Ashburner, R. S. Frackowiak, C. D. Frith, Navigation-related structural change in the hippocampi of taxi drivers. *Proc. Natl. Acad. Sci. U.S.A.* **97**, 4398–4403 (2000). Medline doi:10.1073/pnas.070039597

42. T. Hartley, E. A. Maguire, H. J. Spiers, N. Burgess, The well-worn route and the path less traveled: Distinct neural bases of route following and wayfinding in humans. *Neuron* **37**, 877–888 (2003). Medline doi:10.1016/S0896-6273(03)00095-3

43. M. Hirshhorn, C. Grady, R. S. Rosenbaum, G. Winocur, M. Moscovitch, Brain regions involved in the retrieval of spatial and episodic details associated with a familiar environment: An fMRI study. *Neuropsychologia* **50**, 3094–3106 (2012). Medline doi:10.1016/j.neuropsychologia.2012.08.008

44. L. Nadel, S. Hoscheidt, L. R. Ryan, Spatial cognition and the hippocampus: The anterior-posterior axis. *J. Cogn. Neurosci.* **25**, 22–28 (2013). Medline doi:10.1162/jocn_a_00313

45. D. M. Bannerman, R. Sprengel, D. J. Sanderson, S. B. McHugh, J. N. Rawlins, H. Monyer, P. H. Seeburg, Hippocampal synaptic plasticity, spatial memory and anxiety. *Nat. Rev. Neurosci.* **15**, 181–192 (2014). Medline doi:10.1038/nrn3677

46. P. Berens, CircStat: A Matlab toolbox for circular statistics. *J. Stat. Softw.* **31**, 10 (2009). doi:10.18637/jss.v031.i10

47. J. L. Woodard, S. T. Grafton, J. R. Votaw, R. C. Green, M. E. Dobraski, J. M. Hoffman, Compensatory recruitment of neural resources during overt rehearsal of word lists in Alzheimer's disease. *Neuropsychology* **12**, 491–504 (1998). Medline doi:10.1037/0894-4105.12.4.491

48. C. L. Grady, A. R. McIntosh, S. Beig, M. L. Keightley, H. Burian, S. E. Black, Evidence from functional neuroimaging of a compensatory prefrontal network in Alzheimer's disease. *J. Neurosci.* **23**, 986–993 (2003). Medline

49. M. W. Bondi, W. S. Houston, L. T. Eyler, G. G. Brown, fMRI evidence of compensatory mechanisms in older adults at genetic risk for Alzheimer disease. *Neurology* **64**, 501–508 (2005). Medline doi:10.1212/01.WNL.0000150885.00929.7E

50. C. Rosano, H. J. Aizenstein, J. L. Cochran, J. A. Saxton, S. T. De Kosky, A. B. Newman, L. H. Kuller, O. L. Lopez, C. S. Carter, Event-related functional magnetic resonance imaging investigation of executive control in very old individuals with mild cognitive impairment. *Biol. Psychiatry* **57**, 761–767 (2005). Medline doi:10.1016/j.biopsych.2004.12.031

51. S. D. Han, W. S. Houston, A. J. Jak, L. T. Eyler, B. J. Nagel, A. S. Fleisher, G. G. Brown, J. Corey-Bloom, D. P. Salmon, L. J. Thal, M. W. Bondi, Verbal paired-associate learning by APOE genotype in non-demented older adults: fMRI evidence of a right hemispheric compensatory response. *Neurobiol. Aging* **28**, 238–247 (2007). Medline doi:10.1016/j.neurobiolaging.2005.12.013

52. C. E. Wierenga, N. H. Stricker, A. McCauley, A. Simmons, A. J. Jak, Y. L. Chang, L. Delano-Wood, K. J. Bangen, D. P. Salmon, M. W. Bondi, Increased functional brain response during word retrieval in cognitively intact older adults at genetic risk for Alzheimer's disease. *Neuroimage* **51**, 1222–1233 (2010). Medline doi:10.1016/j.neuroimage.2010.03.021

53. N. A. Suthana, A. Krupa, M. Donix, A. Burggren, A. D. Ekstrom, M. Jones, L. M. Ercoli, K. J. Miller, P. Siddarth, G. W. Small, S. Y. Bookheimer, Reduced hippocampal CA2, CA3, and dentate gyrus activity in asymptomatic people at genetic risk for Alzheimer's disease. *Neuroimage* **53**, 1077–1084 (2010). Medline doi:10.1016/j.neuroimage.2009.12.014

54. C. R. Mondadori, A. Buchmann, H. Mustovic, C. F. Schmidt, P. Boesiger, R. M. Nitsch, C. Hock, J. Streffer, K. Henke, Enhanced brain activity may precede the diagnosis of Alzheimer's disease by 30 years. *Brain* **129**, 2908–2922 (2006). Medline doi:10.1093/brain/awl266

55. B. C. Dickerson, D. H. Salat, D. N. Greve, E. F. Chua, E. Rand-Giovannetti, D. M. Rentz, L. Bertram, K. Mullin, R. E. Tanzi, D. Blacker, M. S. Albert, R. A. Sperling, Increased hippocampal activation in mild cognitive impairment compared to normal aging and AD. *Neurology* **65**, 404–411 (2005). Medline doi:10.1212/01.wnl.0000171450.97464.49

56. K. A. Celone, V. D. Calhoun, B. C. Dickerson, A. Atri, E. F. Chua, S. L. Miller, K. DePeau, D. M. Rentz, D. J. Selkoe, D. Blacker, M. S. Albert, R. A. Sperling, Alterations in memory networks in mild cognitive impairment and Alzheimer's disease: An independent component analysis. *J. Neurosci.* **26**, 10222–10231 (2006). Medline doi:10.1523/JNEUROSCI.2250-06.2006

57. Y. T. Quiroz, A. E. Budson, K. Celone, A. Ruiz, R. Newmark, G. Castrillón, F. Lopera, C. E. Stern, Hippocampal hyperactivation in presymptomatic familial Alzheimer's disease. *Ann. Neurol.* **68**, 865–875 (2010). Medline doi:10.1002/ana.22105

58. D. Putcha, M. Brickhouse, K. O'Keefe, C. Sullivan, D. Rentz, G. Marshall, B. Dickerson, R. Sperling, Hippocampal hyperactivation associated with cortical thinning in Alzheimer's disease signature regions in non-demented elderly adults. *J. Neurosci.* **31**, 17680–17688 (2011). Medline doi:10.1523/JNEUROSCI.4740-11.2011

59. W. Huijbers, E. C. Mormino, A. P. Schultz, S. Wigman, A. M. Ward, M. Larvie, R. E. Amariglio, G. A. Marshall, D. M. Rentz, K. A. Johnson, R. A. Sperling, Amyloid-β deposition in mild cognitive impairment is associated with increased hippocampal activity, atrophy and clinical progression. *Brain* **138**, 1023–1035 (2015). Medline doi:10.1093/brain/awv007

60. W. J. Jagust, E. C. Mormino, Lifespan brain activity, β-amyloid, and Alzheimer's disease. *Trends Cogn. Sci.* **15**, 520–526 (2011). Medline doi:10.1016/j.tics.2011.09.004

61. C. F. Doeller, N. Burgess, Distinct error-correcting and incidental learning of location relative to landmarks and boundaries. *Proc. Natl. Acad. Sci. U.S.A.* **105**, 5909–5914 (2008). Medline doi:10.1073/pnas.0711433105

62. S. H. Yun, K. A. Park, P. Sullivan, J. F. Pasternak, M. J. Ladu, B. L. Trommer, Blockade of nicotinic acetylcholine receptors suppresses hippocampal long-term potentiation in wild-type but not ApoE4 targeted replacement mice. *J. Neurosci. Res.* **82**, 771–777 (2005). Medline doi:10.1002/jnr.20684

3. Danksagung

Die vorliegende Arbeit entstand während meiner Zeit als Doktorand in der Klinik für Epileptologie des Universitätsklinikums Bonn und am Deutschen Zentrum für Neurodegenerative Erkrankungen (DZNE), Bonn. An dieser Stelle möchte ich mich bei allen Personen bedanken, die zu ihrem erfolgreichen Gelingen beigetragen haben.

Zunächst bedanke ich mich herzlich bei meinen beiden Doktorvätern Herr Prof. Dr. Nikolai Axmacher und Herr PD Dr. Jürgen Fell für die freundliche Überlassung des Themas sowie die fachliche und materielle Förderung meines Forschungsvorhabens. Herr Prof. Dr. Nikolai Axmacher und Herr PD Dr. Jürgen Fell standen mir jederzeit für fachliche und menschliche Unterstützung zur Verfügung und bestärkten meine Freude am experimentellen Arbeiten. Durch ihren steten Ansporn, ihre Begeisterungsfähigkeit, ihre Herzlichkeit und ihr offenes Ohr haben sie das Gelingen dieser Arbeit ermöglicht. Ich möchte mich ebenfalls bei Herrn Prof. Dr. Christian E. Elger und Herrn Prof. Dr. Thomas Klockgether für die materielle Unterstützung meines Forschungsprojekts bedanken.

Besonderer Dank richtet sich ferner an meine Kooperationspartner vom Donders Institute for Brain, Cognition and Behaviour der Radboud-Universität Nijmegen Herr Prof. Dr. Christian Doeller und Herr Dr. Tobias Navarro Schröder, meine Kooperationspartner aus dem Institut für Psychologie der Universität Bonn Herr Prof. Dr. Christian Montag, Herr Prof. Dr. Martin Reuter, Herr Bernd Lachmann und Frau Rayna Sariyska, meine Mitarbeiter aus der Klinik für Epileptologie der Universität Bonn Frau Dr. Hui Zhang, Frau Dr. Lorena Deuker, Frau Dr. Carina Oehrn, Herr Dr. Marcin Leszczynski, Frau Dr. Leila Chaieb und Herr Dr. Thomas Reber sowie meine Mitarbeiter am Deutschen Zentrum für Neurodegenerative Erkrankungen Herr Prof. Dr. Tony Stöcker, Herr Dr. Rüdiger Stirnberg, Frau Dr. Hweeling Lee, Frau Dr. Verena Heise, Herr Paul Christian Messing-Flöter, Frau Anke Rühling und Herr Yilmaz Sagik.

Des Weiteren gilt mein Dank der Studienstiftung des deutschen Volkes und dem SciMed Promotionskolleg der Medizinischen Fakultät der Universität Bonn für die materielle und ideelle Förderung der Arbeit.